Impacts of Tropical North Atlantic and Equatorial Atlantic SST Anomalies on ENSO

LEISHAN JIANG[a,b] AND TIM LI[b,a]

[a] Key Laboratory of Meteorological Disaster, Ministry of Education/Joint International Research Laboratory of Climate and Environmental Change/Collaborative Innovation Center on Forecast and Evaluation of Meteorological Disasters (CIC-FEMD), Nanjing University of Information Science and Technology, Nanjing, China
[b] Department of Atmospheric Sciences, University of Hawai'i at Mānoa, Honolulu, Hawaii

(Manuscript received 29 October 2020, in final form 1 April 2021)

ABSTRACT: The sea surface temperature anomaly (SSTA) in the tropical Atlantic during boreal spring and summer shows two dominant modes: a basin-warming mode and a meridional dipole mode, respectively. Observational and coupled model simulations indicate that the former induces a Pacific La Niña in the succeeding winter whereas the latter cannot. The basin-warming forcing induces a La Niña through a Kelvin wave response and the associated wind–evaporation–SST–convection (WESC) feedback over the northern Indian Ocean (NIO) and Maritime Continent (MC). An anomalous Kelvin wave easterly interacts with the monsoonal westerly, leading to a warm SSTA and a northwest–southeast-oriented heating anomaly in NIO/MC, which further induces easterly and cold SSTAs over the equatorial Pacific. In contrast, the dipole forcing has little impact on the Indian and Pacific Oceans due to the offsetting of the Kelvin wave to the asymmetric Atlantic heating. Further observational and modeling studies of the tropical North Atlantic (TNA) and equatorial Atlantic (EA) SSTA modes indicate that the TNA (EA) forcing induces a CP-type (EP-type) ENSO. In both cases, the Kelvin wave response and the WESC feedback over the NIO/MC are important in conveying the Atlantic's impact. The difference lies in distinctive Rossby wave responses: a marked westerly anomaly appears in the equatorial eastern Pacific (EEP) for the TNA forcing (due to its westward location) while no significant wind response is observed in the EEP for the EA forcing. The westerly anomaly prevents a cooling tendency in the EEP through anomalous zonal and vertical advection according to a mixed layer heat budget analysis.

KEYWORDS: Atlantic Ocean; ENSO; Teleconnections; Atmosphere-ocean interaction; Climate models; Interannual variability

1. Introduction

El Niño–Southern Oscillation (ENSO) is the most dominant mode on the interannual time scale in the Pacific, which can excite atmospheric teleconnections to influence global weather and climate (Horel and Wallace 1981; Philander 1983). Many previous studies pointed out that ENSO could exert a significant impact on the tropical Atlantic sea surface temperature anomaly (SSTA) variability through either a tropical or a midlatitude teleconnection process (Enfield and Mayer 1997; Klein et al. 1999; Saravanan and Chang 2000; Alexander and Scott 2002; Chiang and Sobel 2002; Chang et al. 2006; Lee et al. 2008; Lübbecke and McPhaden 2012; Richter et al. 2013; Park and Li 2018; Jiang and Li 2019; Wu and He 2019; Wu et al. 2020). Previous studies (e.g., Ding et al. 2012; Ham et al. 2013a; Keenlyside et al. 2013; Polo et al. 2015; Wang et al. 2017) also suggested that the tropical Atlantic variability, especially the tropical North Atlantic (TNA) and equatorial Atlantic (EA) SSTA, could feed back to the Pacific ENSO variability and could be used as an additional predictor to improve ENSO prediction. Therefore, understanding how the tropical Atlantic affects the Pacific is crucial to understand the tropical interbasin teleconnection (Cai et al. 2019) and to predict ENSO and its global impacts.

Processes through which the TNA SSTA affects the Pacific climate may be separated into two groups (Li et al. 2017). One is through the Rossby wave response to the west of the anomalous heat source over the TNA (Ham et al. 2013a,b; Wang et al. 2017). The other is via the Kelvin wave response to the east of the anomalous heat source over the TNA (Rong et al. 2010; Yu et al. 2016).

Ham et al. (2013a) suggested that a March–May (MAM) TNA warming could serve as a trigger for the subsequent wintertime La Niña event. In brief, a MAM TNA warming would induce a positive heating anomaly over the Atlantic intertropical convergence zone (ITCZ), which would generate a low-level cyclonic circulation anomaly to the west as a Rossby wave response. A northerly anomaly in the western flank of the anomalous cyclone enhances the trade wind over the northeastern Pacific, leading to a cold SSTA there. This cooling effect, together with the atmospheric cold and dry advection, induces suppressed convection in situ and a low-level anticyclonic flow to its west. An easterly anomaly in the southern flank of the anticyclone acts as a trigger for the occurrence of La Niña by inducing upwelling Kelvin wave propagating eastward. However, as pointed out by Ham and Kug (2015), in CMIP3 and CMIP5 models the TNA-induced Rossby wave process over the subtropical northeastern Pacific is weak and undetected. Therefore, there is a need to re-examine the Rossby wave effect.

Supplemental information related to this paper is available at the Journals Online website: https://doi.org/10.1175/JCLI-D-20-0835.s1.

Corresponding author: Tim Li, timli@hawaii.edu

DOI: 10.1175/JCLI-D-20-0835.1

In addition to the Rossby wave process, the Kelvin wave process is also suggested. Rong et al. (2010) pointed out that the MAM TNA SSTA may act as a ''bridge'' to link the preceding wintertime ENSO to East Asian monsoon in subsequent summer through the TNA-induced atmospheric easterly Kelvin wave, which can generate anticyclonic shear over the western North Pacific (WNP). Besides, Yu et al. (2016) proposed an ''Indian Ocean relay effect,'' which highlights the role of the Indian Ocean in conveying the impact from the tropical Atlantic to the Pacific. Their results show that the cold SSTA in TNA can induce anomalous low-level westerly in the tropical Indian Ocean as a Kelvin wave response and this anomalous westerly flow superimposes on the mean westerly in the northern Indian Ocean (NIO) during boreal summer, increasing local surface wind speed and surface evaporation to cool the SST in situ. A cold SSTA in the NIO further suppresses local convection, inducing anomalous westerlies to its east as a Kelvin wave response, leading to enhanced cyclonic vorticity over the WNP monsoon trough region to favor the tropical cyclone genesis.

Besides, the equatorial Atlantic SSTA (also called Atlantic Niño; Zebiak 1993; Carton and Huang 1994) may also influence the ENSO evolution in subsequent seasons. The EA mode is one of the dominant interannual modes in the tropical Atlantic basin and is characterized by a significant SSTA over the cold tongue region with maximum variability during boreal summer [June–August (JJA)] (Keenlyside and Latif 2007; Xie and Carton 2013). Previous studies pointed out that the EA SSTA has had a robust influence on ENSO since the 1970s with a statistically significant negative correlation when the equatorial Atlantic index leads the ENSO index by approximately six months (Keenlyside and Latif 2007; Polo et al. 2008; Rodríguez-Fonseca et al. 2009; Ding et al. 2012; Polo et al. 2015). A descent anomaly appeared in the equatorial central Pacific (near the date line) in response to the EA SSTA forcing, and it was hypothesized that this Atlantic impact was through an anomalous Walker circulation (Rodríguez-Fonseca et al. 2009; Ding et al. 2012; Polo et al. 2015). This raises an issue of what determines the horizontal length scale of the Walker circulation. According to Gill (1980), the horizontal length scale of a Rossby wave response to the west of a heat source is 3 times shorter than that of a Kelvin wave response to the east. Therefore, if an anomalous descent over the Maritime Continent is viewed as a direct Rossby wave–induced Walker circulation response to El Niño heating over the date line with a longitudinal distance of 60°, it is unphysical to assume that the descent over the date line is a direct Rossby wave–induced Walker circulation response to the EA forcing given that the longitudinal distance is 2–3 times larger. The argument above is supported by a Gill model simulation (Figs. S1a,b in the online supplemental material), which shows that the Rossby wave response to the EA heating is mostly confined in the South America continent with a low-level divergence over 90°W, which is far away from the central Pacific. The full-physics atmospheric general circulation model (ECHAM4) simulation (Figs. S1c,d) further shows that due to the moderate magnitude of the EA forcing, the easterly wind associated with the Kelvin wave response is mostly confined in the tropical Indian Ocean and the anomalous divergence over the central Pacific is negligible. This motivates us to investigate specific processes through which the equatorial Atlantic heating affects circulation in the Pacific.

It has been suggested that the TNA and EA SSTA modes may favor the development of a central Pacific (CP) and an eastern Pacific (EP) type of ENSO in subsequent seasons, respectively (Ham et al. 2013b), but the physical mechanisms through which the Atlantic modes affect the ENSO evolution are unclear. While most of the previous studies examined the composite TNA or EA SSTA impacts, in reality these two SSTA patterns may coexist, either with the same sign or an opposite sign. This motivates us to further examine the basinwide SSTA modes in the tropical Atlantic in addition to the TNA and EA indices.

The overall objective of the current study is to re-examine the impacts of basinwide SSTA modes and individual TNA and EA indices on the Pacific ENSO evolution and pattern diversity and to reveal the physical mechanisms through which the different Atlantic SSTA modes affect the wind and SST in the tropical Pacific.

The remaining part of the paper is organized as the following. Section 2 describes the datasets, methods, and models used in this study. Section 3 shows the impacts of the tropical Atlantic basinwide SSTA modes on ENSO. The impacts of the composite TNA and EA SSTA patterns on subsequent ENSO evolution and pattern diversity are examined in section 4. A discussion section is presented in section 5, and conclusions are given in section 6.

2. Data, methods, and numerical experiments

a. Data and methods

The datasets used in this study include 1) monthly precipitation data from the Global Precipitation Climatology Project (GPCP; Adler et al. 2003); 2) monthly SST data from the Hadley Centre Global Sea Ice and Sea Surface Temperature (HadISST; Rayner et al. 2003); and 3) monthly horizontal winds from National Centers for Environment Prediction (NCEP)–Department of Energy (DOE) AMIP II reanalysis (NCEP2; Kanamitsu et al. 2002).

To determine the leading patterns of interannual SST variability over the tropical Atlantic (30°S–30°N, 70°W–20°E) during 1981–2018, empirical orthogonal function (EOF) analysis is applied to decompose the spatiotemporal SSTA into orthogonal modes in terms of EOF patterns, and each EOF pattern is associated with a principal component (PC) time series, which describes the temporal evolution of the EOF patterns. To further identify the impact of the Atlantic leading EOF modes on subsequent ENSO evolution while attempting to remove the oscillatory effect of ENSO itself, a linear lagged partial regression analysis is applied to show the linear relationship between the normalized PCs and the subsequent Pacific circulations after excluding the possible influence of the preceding wintertime Niño-3.4 (5°S–5°N, 170°–120°W) SSTA, following Saji and Yamagata (2003) and Ham et al. (2013a). Moreover, to understand the physical processes that cause the

TABLE 1. List of numerical experiments conducted by CESM1.2.2. Positive and negative forcing added in the model are exactly in mirror image.

Experiments		Description	Integration time
EXP_ATL_CTRL		The Atlantic basin within 50°S–50°N is prescribed with the observed climatological mean SST annual cycle averaged during 1980–2010, and the ocean and atmosphere is freely coupled elsewhere.	Integrating continuously for 100 years.
EXP_EOF1	EXP_EOF1(+) EXP_EOF1(−)	The tropical Atlantic (30°S–30°N, 70°W–20°E) is prescribed with positive (negative) phase of EOF-1 SST anomaly pattern plus observed climatological SST annual cycle. The configuration for the remaining regions is the same as the EXP_ATL_CTRL.	The SST anomaly patterns added for these eight sensitivity experiments are from 1 Mar to 31 Sep each year, and each experiment is repeated for 30 times with different initial condition obtained randomly from the EXP_ATL_CTRL.
EXP_EOF2	EXP_EOF2(+) EXP_EOF2(−)	The tropical Atlantic (30°S–30°N, 70°W–20°E) is prescribed with positive (negative) phase of EOF-2 SST anomaly pattern plus observed climatological SST annual cycle. The configuration for the remaining regions is the same as the EXP_ATL_CTRL.	
EXP_TNA	EXP_TNA(+) EXP_TNA(−)	The tropical Atlantic (30°S–30°N, 70°W–20°E) is prescribed with composite positive (negative) TNA SST anomaly pattern plus observed climatological SST annual cycle. The configuration for the remaining regions is the same as the EXP_ATL_CTRL.	
EXP_EA	EXP_EA(+) EXP_EA(−)	The tropical Atlantic (30°S–30°N, 70°W–20°E) is prescribed with composite positive (negative) EA SST anomaly pattern plus observed climatological SST annual cycle. The configuration for the remaining regions is the same as the EXP_ATL_CTRL.	

SSTA change over a certain region, a mixed layer budget analysis is also applied following Chen et al. (2016).

For the significance test, a two-tailed Student's t test is adopted for composite analysis and an F test is used for partial regression analysis. The confidence level in this study is 95%. Moreover, the TNA index is defined as the SST anomalies averaged over 5°–25°N, 70°–10°W and the EA (or Atl3) index is defined as the SST anomalies averaged over 4°S–4°N, 20°W–0°.

b. *Numerical experiments*

As the statistical partial regression analysis may not be able to eliminate the influence of the preceding ENSO effect completely due to the different temporal evolution features of ENSO and the sample size problem, partially coupled model experiments are designed to examine the pure impact of the Atlantic forcing on the Pacific. The coupled general circulation model (CGCM) adopted in this study is the Community Earth System Model (CESM) version 1.2.2 that is developed by the National Center for Atmospheric Research (NCAR) (Hurrell et al. 2013). Its atmospheric component is the Community Atmosphere Model (CAM) version 4 (Neale et al. 2013), and the oceanic component is an extension of the Parallel Ocean Program (POP), version 2 (Smith et al. 2010). The horizontal resolution for the atmospheric model is 0.9° latitude × 1.25° longitude and for the oceanic model is an irregular grid (approximately 0.58° × 0.58°).

In some previous studies (Ham et al. 2013b; Ding et al. 2012; Polo et al. 2015), they apply the partially coupled "time-series pacemaker experiment" (Kosaka and Xie 2013) in which the Atlantic basin is specified with the observed time evolution of SST pattern from one period (e.g., 1979–2017) whereas other regions are freely coupled. However, one limitation of this type of pacemaker experiment in analyzing the pure impact of the Atlantic SSTA on the Pacific is that the preceding ENSO effect still needs to be removed by partial-regression analysis. Therefore, in this study, to avoid the influence of the preceding ENSO signal, we apply the "idealized pacemaker experiment" (Ham et al. 2013a; Ruprich-Robert et al. 2017; Wu and He 2019) in which a composite SST pattern is prescribed in one region and do ensemble simulations with different initial conditions.

Table 1 lists one control experiment and four sets of sensitivity experiments designed for this study. The control experiment

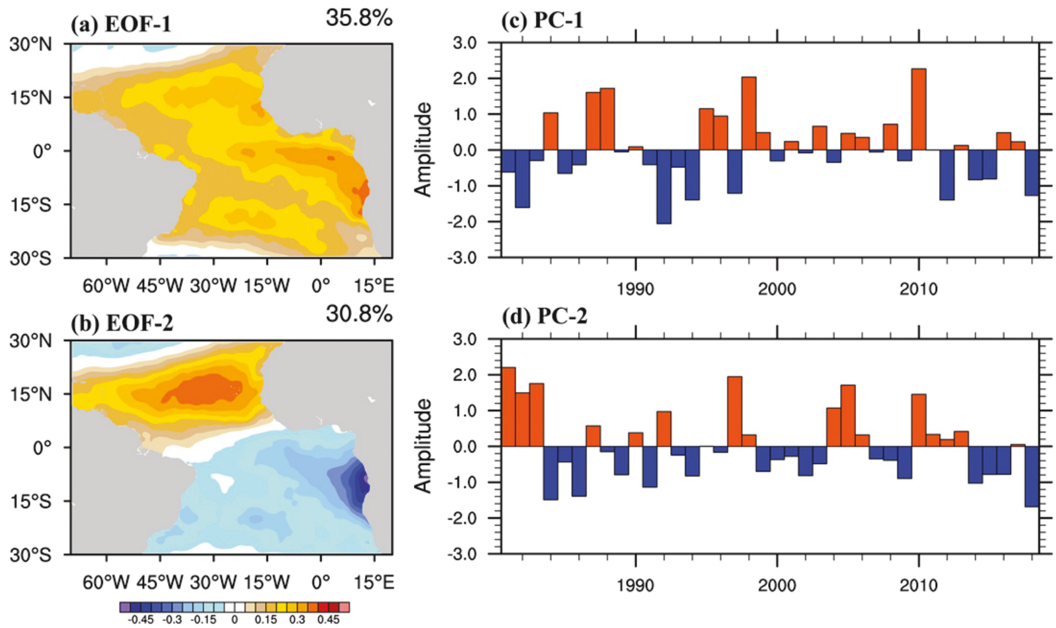

FIG. 1. The empirical orthogonal function (EOF) analysis of detrended MAMJJA (March–August) tropical Atlantic (30°S–30°N, 70°W–20°E) sea surface temperature anomaly during 1981–2018. (a),(b) The first and second EOF modes (°C). (c),(d) The corresponding normalized principal components (PCs) of EOF-1 and EOF-2.

(EXP_ATL_CTRL) denotes that the Atlantic basin within 50°S–50°N is prescribed with the observed climatological mean annual cycle during 1980–2010 whereas the ocean and atmosphere is freely coupled elsewhere. Observed SST climatology instead of the model climatology is nudged into the model for control run is because the model exhibits a cold (warm) SST bias in the tropical North Atlantic (Atlantic cold tongue) region, which is a common problem for most CGCMs (Richter et al. 2012; Xu et al. 2014; Lübbecke et al. 2018; Wang et al. 2014). The control experiment is integrated continuously for 100 years, and we have randomly adopted 30 years as the reference years for the following sensitivity experiments. In the second (EXP_EOF1) and third (EXP_EOF2) experiments, the SSTA patterns derived from the observational EOF analysis, namely the EOF-1 and EOF-2 patterns, are added on the observed climatological mean annual cycle in the tropical Atlantic (30°S–30°N, 70°W–20°E), respectively and the configuration for the remaining regions are the same as the control run (EXP_ATL_CTRL). The temporal evolution for EOF patterns added in the model is obtained through a lead–lag regression toward the associated normalized PC series. The configurations for the fourth (EXP_TNA) and fifth (EXP_EA) experiments are the same as the previous two sensitivity experiments except that the prescribed SST anomaly patterns are derived from the composite TNA warming (1981, 1983, 1987, 1988, 1998, 2005, 2010) and EA warming (1984, 1987, 1988, 1995, 1996, 1998, 1999, 2008, 2010) events. Meanwhile, for each set of sensitivity experiments above, both the positive forcing and negative forcing experiments are conducted and the negative forcing added is simply opposite to the positive forcing. For example, the EXP_TNA contains two subexperiments with TNA warming forcing [EXP_TNA (+)] and TNA cooling forcing [EXP_TNA(−)]. Therefore, the total will be eight sensitivity experiments. The SSTA patterns added for the above sensitivity experiments are from 1 March to 31 September each year, and each experiment is repeated 30 times with different initial conditions obtained from the control run. To maximum the signal-to-noise ratio, the model simulation results shown below are the ensemble mean of the difference between the positive forcing experiment and negative forcing experiment among 30 ensemble members [e.g., EXP_TNA (+) minus EXP_TNA(−) divided by two].

3. Impacts of tropical Atlantic basin SSTA modes on ENSO evolution

Several studies (e.g., Rodríguez-Fonseca et al. 2009; Ding et al. 2012; Ham et al. 2013a,b; Polo et al. 2015) have verified the impact of the TNA/EA SSTA modes on the Pacific through observational analysis and numerical simulations. However, these two SSTA patterns may coexist, either with the same sign or an opposite sign. Therefore, as the first step, we investigate the evolution patterns of the dominant Atlantic basinwide SSTA modes during their most active (boreal spring and summer) seasons and the physical mechanisms through which these basinwide modes affect the ENSO in subsequent seasons.

a. Observational analyses

First, an EOF analysis is conducted to extract the leading modes of SST variability in the tropical Atlantic. As the TNA SSTA usually peaks during MAM while the EA SSTA reaches

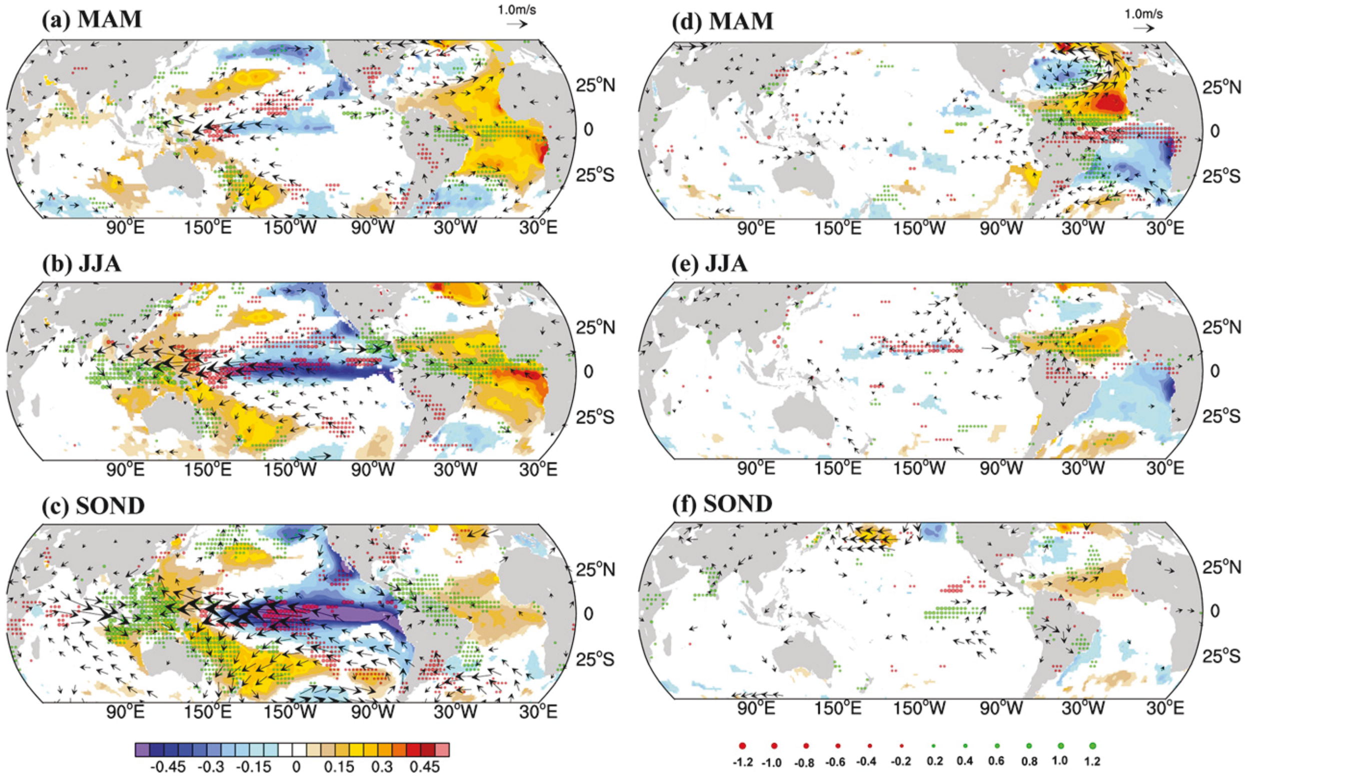

FIG. 2. Lagged partial-regression analysis of (a) MAM, (b) JJA, and (c) September–December (SOND) SST (shading; °C), 850-hPa wind (vectors; m s^{-1}), and precipitation (dots; mm day^{-1}) on normalized PC-1 during 1981–2018 by excluding the effect of preceding January–February (JF) Niño-3.4 index. (d)–(f) As in (a)–(c), but for regression on normalized PC-2. Only the values above the 95% confidence level are plotted.

its maximum amplitude during JJA, the MAMJJA (March–August) averaged SSTA is used to obtain the leading patterns of the tropical Atlantic. Figures 1a and 1b show the first and second EOF modes of detrended MAMJJA SSTA in the tropical Atlantic (30°S–30°N, 70°W–20°E). The first (second) leading EOF mode, which accounts for 35.8% (30.8%) of the variance, exhibits a basinwide (meridional dipole) SSTA pattern with an in-phase (out-of-phase) relationship between the tropical North Atlantic and equatorial South Atlantic. The normalized principal components associated with these two leading EOF modes are shown in Figs. 1c and 1d. Both PC-1 and PC-2 vary on the interannual time scale.

To further examine the impacts of EOF-1 (basin-warming mode) and EOF-2 (north–south dipole mode) on subsequent ENSO evolution, a lagged partial-regression analysis is conducted with respect to the normalized PC-1 (Figs. 2a–c) and PC-2 (Figs. 2d–f) by excluding the effect of preceding JF (January–February) Niño-3.4 SSTA. One prominent feature in Fig. 2 is that the basin-warming forcing is accompanied by a significant La Niña event in subsequent winter (Fig. 2c) while the meridional dipole forcing (Fig. 2f) is not. During MAM, for basin-warming forcing, the tropical Atlantic ITCZ shows uniform positive precipitation anomaly (Fig. 2a) in response to the basin-warming SSTA, which excites a cyclonic Rossby wave response over the subtropical northeastern Pacific as a Gill-type response (Gill 1980). This cyclonic circulation is regarded as the critical system in conveying the Atlantic's impact to the Pacific by inducing cold SSTA and negative heating over the subtropical northeastern Pacific as proposed by Ham et al. (2013a). For meridional dipole forcing, the tropical Atlantic heating exhibits a dipole pattern (Fig. 2d) and in response to this dipole heating, two pairs of cyclonic Rossby wave circulations occur over the eastern Pacific and the northern counterpart is associated with the cold SSTA over the subtropical northeastern Pacific (Fig. 2d).

During JJA, for basin-warming forcing, the tropical Atlantic positive rainfall anomaly associated with the cyclonic Rossby wave response is strengthened (Fig. 2b), which tends to amplify the coupling among northerly wind, cold SSTA, and negative rainfall anomaly over the subtropical northeastern Pacific. This negative heating would further enhance the easterly response over the EWP by inducing an anticyclonic Rossby wave circulation to its west. Meanwhile, it is interesting to note that warm SSTA appears over the surrounding region of the Maritime Continent and positive rainfall anomaly extends from the northern Indian Ocean (NIO) to the Maritime Continent (MC) (Fig. 2b), which is supposed to induce a Kelvin wave to the east to enhance the easterly anomaly over the EWP. This local warm SSTA may arise partly from the interaction between the easterly Kelvin wave and mean westerly as illustrated by Yu et al. (2016). However, for the meridional dipole forcing, the rainfall anomaly pattern over the tropical Atlantic is still a dipole structure during JJA, and the Kelvin wave response to the east and its associated air–sea interaction over the NIO/MC are negligible (Fig. 2e), which is not sufficient to induce easterly anomaly over the EWP. It is worth noting that the northerly wind on the western flank of the cyclonic Rossby wave circulation is strengthened associated with cold SST and negative rainfall anomaly over the subtropical northeastern Pacific (Fig. 2e). However, the negative heating eventually only remains in the off-equatorial region (around 10°N) and fails to induce a significant easterly anomaly over the EWP and La Niña event afterward (Fig. 2f).

The discussion above suggests that both basin-warming forcing (Figs. 2a,b) and meridional dipole forcing (Figs. 2d,e) can generate a Rossby wave response over the subtropical northeastern Pacific. However, the easterly anomaly over the EWP is only significant for basin-warming forcing but negligible for dipole forcing, and this easterly anomaly plays a crucial role in generating cold SSTA over the central-eastern Pacific by inducing upwelling Kelvin wave propagating eastward. One hypothesis for the cause of this significant (insignificant) zonal wind response over the EWP to the basin-warming (meridional dipole) forcing is that the Atlantic-induced Kelvin wave process to the east is strong (negligible). For basin-warming forcing, the uniform Atlantic positive heating could induce significant easterly Kelvin wave to the east, which may interact with the mean monsoonal westerly circulation over the NIO/MC to induce warm SSTA and positive heating anomaly in suit. This positive heating may further enhance the easterly anomaly over the EWP to trigger La Niña. However, for meridional dipole forcing, the Kelvin wave response would be much weaker due to the cancellation effect to the asymmetric dipole heating and the Kelvin wave–induced air–sea interaction over the NIO/MC may also be too weak to induce easterly anomaly over the EWP.

In the following subsection, the idealized coupled model experiments are designed to investigate whether the establishment of the Atlantic-induced Kelvin wave process is responsible for the significant (insignificant) impact of basin-warming (meridional dipole) forcing on ENSO evolution.

b. *Idealized coupled model simulations*

As mentioned in section 2b, the observational partial-regression analysis may not completely remove the influence of the preceding ENSO signal due to the different temporal evolution features of ENSO and the sample size problem. In this subsection, idealized partially coupled model experiments are conducted to examine the impacts of the basin-warming and meridional dipole forcing on the Pacific. The SSTA patterns added in the tropical Atlantic for EXP_EOF1 and EXP_EOF2 are derived from the lagged regression analysis of SSTA on normalized PC-1 and PC-2 during 1981–2018. As the composite of normalized PC-1/PC-2 above one standard deviation (Figs. 1c,d) is around 1.8, the SSTA magnitude for the prescribed forcing is multiplied by a factor of 1.8 to attain the realistic amplitude.

Figure S2 shows the time evolution of the model-simulated Niño-3.4 index anomaly for EXP_EOF1 and EXP_EOF2 as the deviation from EXP_ATL_CTRL. The ensemble mean of the 30 members of EXP_EOF1 (+) [EXP_EOF1 (−)] [solid red (blue) line in Fig. S2a] shows a pronounced negative (positive) value, indicating that the multimember ensemble simulation is capable of simulating the opposite impact of the Atlantic positive (negative) forcing on the Pacific. In contrast, the ensemble mean of the Niño-3.4 index simulated by EXP_EOF2 [solid red (blue) line in Fig. S2b] is near zero and there is no clear separation between EXP_EOF2 (+) and EXP_EOF2 (−). To investigate the detailed processes of how the Pacific response to the Atlantic basin-warming forcing and meridional dipole forcing, the spatial–temporal evolutions are illustrated in Fig. 3.

During MAM, for the basin-warming forcing, similar to the observations (Fig. 2a), the tropical Atlantic ITCZ shows a uniformly positive rainfall anomaly (Fig. 3a), and this positive diabatic heating generates a pair of cyclonic Rossby wave to the west and an easterly Kelvin wave to the east extending from the Indian Ocean to the western Pacific. It is noted that theoretically, the amplitude of Kelvin wave always decays away from the forcing region (Gill 1980), while in simulation, the easterly response is larger in the equatorial western Pacific (EWP) than Indian Ocean (Fig. 3a). The detailed evolution shows that the easterly anomaly is originally larger over the tropical Indian Ocean (Fig. 5a) but the easterly anomaly over the EWP is quickly amplified in the following season (Fig. 5b) in response to the significant positive heating (Fig. 5b) over the eastern Maritime Continent, especially near Papua New Guinea. The easterly Kelvin wave superimposes on the model climatological mean westerly (Fig. 4a), reduces wind speed, and increases downward latent heat flux (Fig. 5g) to induce local SSTA warming and positive heating (Fig. 5b). This equatorial positive heating is associated with significant ascending motion (Fig. 5l) near 120°E and could directly generate Kelvin wave to the east to enhance an easterly anomaly over the EWP (Fig. 5b). Moreover, the topographic lifting effect may also contribute to the positive heating over the eastern Maritime Continent. Low-level easterly anomalies associated with the Kelvin wave bump into the narrow and steep high mountain, generating positive convective heating there. In contrast to the observational analysis (Fig. 2a), the cold SSTA associated with the Rossby wave response over the subtropical northeastern Pacific for model simulation is negligible (Fig. 3a; a discussion about this discrepancy will be presented in section 5). For meridional dipole forcing, the rainfall response over the tropical Atlantic exhibits a north–south dipole structure (Fig. 3d). In response to this dipole heating, a cyclonic circulation is excited over the subtropical northeastern Pacific. However, the Kelvin wave response to the dipole heating almost vanishes (Fig. 3d) over the Indian Ocean and western Pacific due to the cancellation of the response to the Atlantic positive heating and negative heating.

During JJA, for basin-warming forcing, to the west, the Rossby wave response is strengthened as the strengthening of the tropical Atlantic heating (Fig. 3b), and a weak cold SSTA is presented over the subtropical northeastern Pacific. The Rossby wave process as illustrated by Ham et al. (2013a) could generate the off-equatorial negative heating over the central North Pacific through inducing cold SSTA and atmospheric

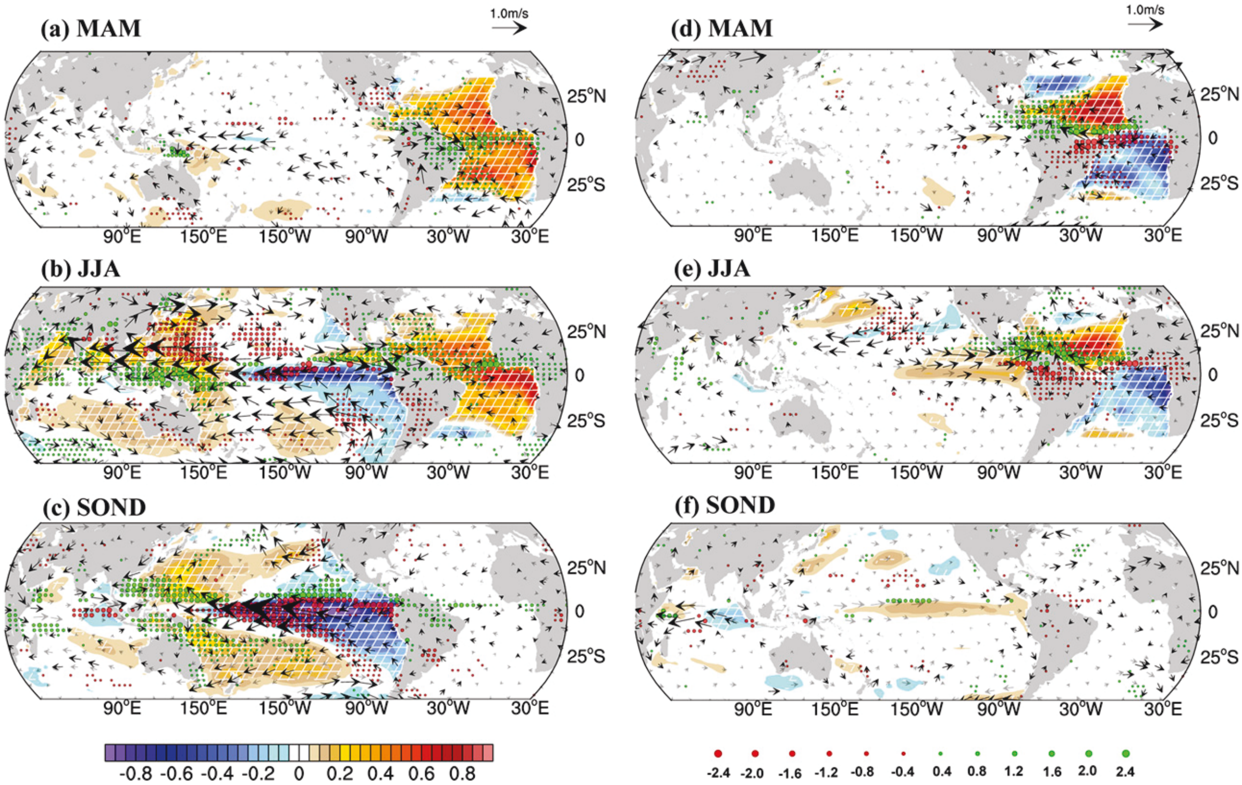

FIG. 3. Spatial evolution of model simulated SST (shading; °C), 850-hPa wind (vectors; m s^{-1}), and precipitation (dots; mm day^{-1}) for the EXP_EOF1 [EXP_EOF1(+) minus EXP_EOF1(−) divided by two] during (a) MAM, (b) JJA, and (c) SOND. (d)–(f) As in (a)–(c), but for the EXP_EOF2. The white hatched area, dotted area, and black vectors indicate above the 95% confidence level.

dry advection (Ham et al. 2013a) and this central North Pacific negative heating could be partly responsible for the easterly anomaly over the EWP by inducing an anticyclonic Rossby wave to the west (Fig. 3b). To the east, it is shown that the significant easterly anomaly associated with the Kelvin wave response extends all the way from the Indian Ocean to the western Pacific, accompanied by the significant SSTA warming and positive heating anomaly over the NIO/MC. This local

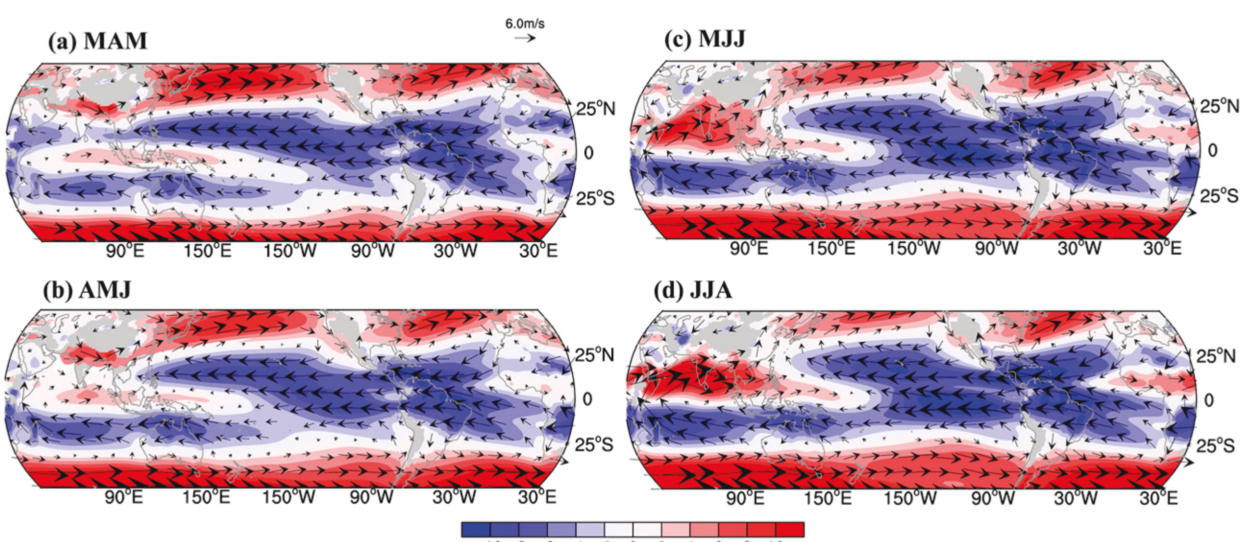

FIG. 4. Model climatological 850-hPa zonal wind (shading; m s^{-1}) and 850-hPa wind (vectors; m s^{-1}) during (a) MAM, (b) AMJ, (c) MJJ, and (d) JJA.

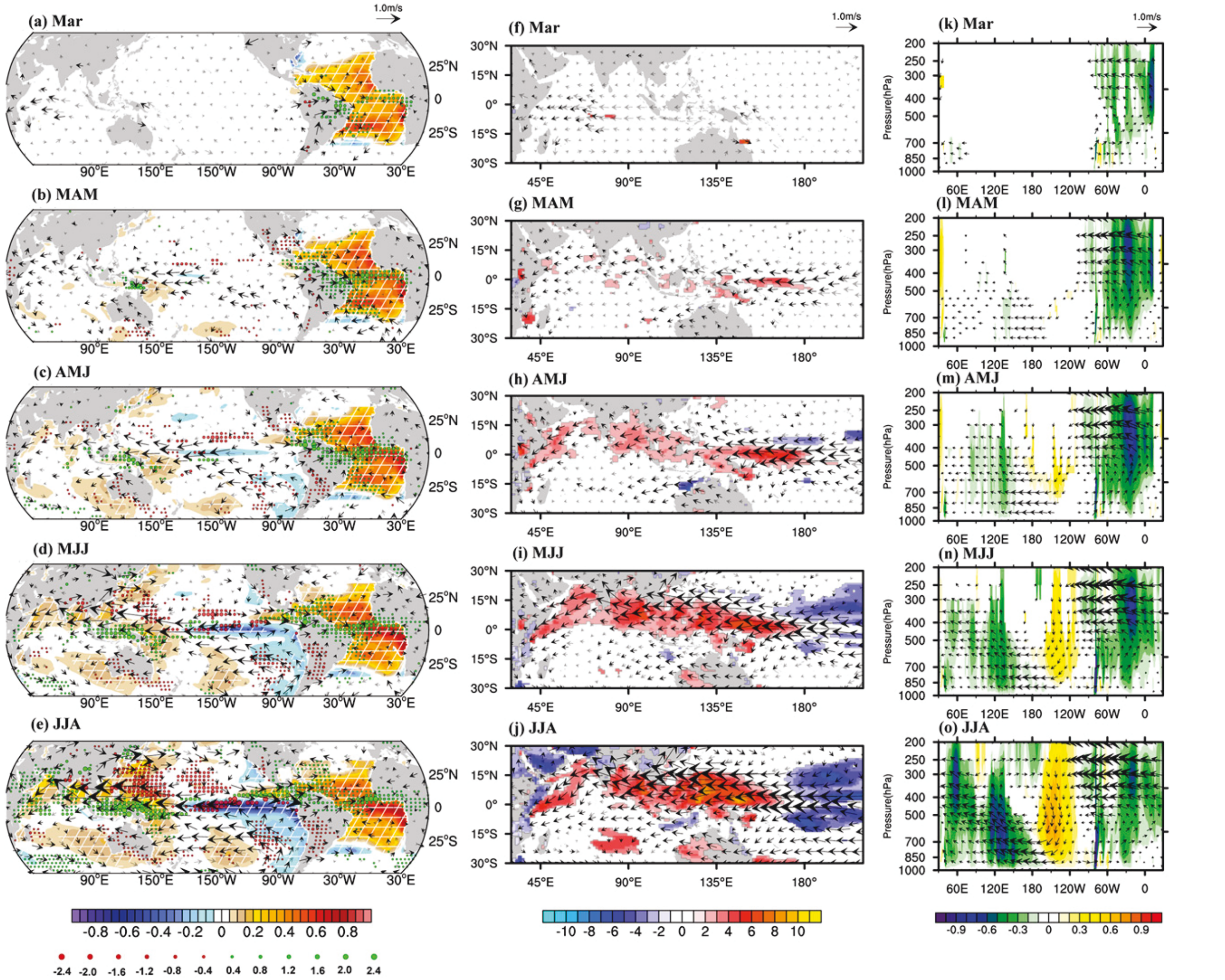

FIG. 5. (a)–(e) Spatial evolution of model simulated SST (shading; °C), 850-hPa wind (vectors; m s^{-1}), and precipitation (dots; mm day^{-1}) for the EXP_EOF1 during March, MAM, AMJ, MJJ, and JJA, respectively. (f)–(j) The model simulated latent heat flux (shading; W m^{-2}; positive downward), 850-hPa wind (vectors; m s^{-1}) during March, MAM, AMJ, MJJ, and JJA, respectively. (k)–(o) Model simulated zonal–vertical cross section of vertical overturning circulation averaged at 8°S–8°N [vectors denote zonal velocity (m s^{-1}) and negative vertical p velocity (Pa s^{-1}); shading denotes anomalous vertical p velocity (Pa s^{-1})] during March, MAM, AMJ, MJJ, and JJA, respectively. The white hatched area in the left column, shaded areas in the right two columns, black vectors, and dots denote the values above the 95% confidence level.

warming could further induce easterly anomaly over the EWP as a Kelvin wave response, which is verified by our AGCM experiments with prescribed SSTA warming over the NIO/MC (Fig. S3). The detailed evolution patterns suggest that the easterly anomaly associated with the Kelvin wave reduces the surface wind speed, increases the downward latent heat flux over the NIO/MC from April–June (AMJ) to JJA (Figs. 5e–g) and leads to the formation of the northwest–southeast-oriented positive SSTA and heating anomaly (Figs. 5b–d) through a wind–evaporation–SST–convection (WESC) feedback. To further verify the Kelvin wave–monsoon interaction over the NIO/MC, a quantitative mixed layer budget analysis (Fig. S4) is conducted for the NIO/MC region during AMJ to reveal the physical processes that causes the SSTA growth. It is shown that the positive mixed layer temperature tendency over the NIO/MC is mainly induced by the increased latent heat flux and that the dynamic terms play very minor roles, which is consistent with our former qualitative analysis. As climate mean state over the Asian monsoon sector is asymmetric (Figs. 4a–d), the easterly response and the Kelvin–monsoon interaction show a stronger component to the north of the equator (Figs. 5a–e). Moreover, it is noted that the off-equatorial negative heating anomalies over the central-western Pacific associated with the easterly-induced anticyclonic shear become stronger during JJA (Figs. 5a–d), and this negative heating may also enhance the easterly anomaly over the EWP

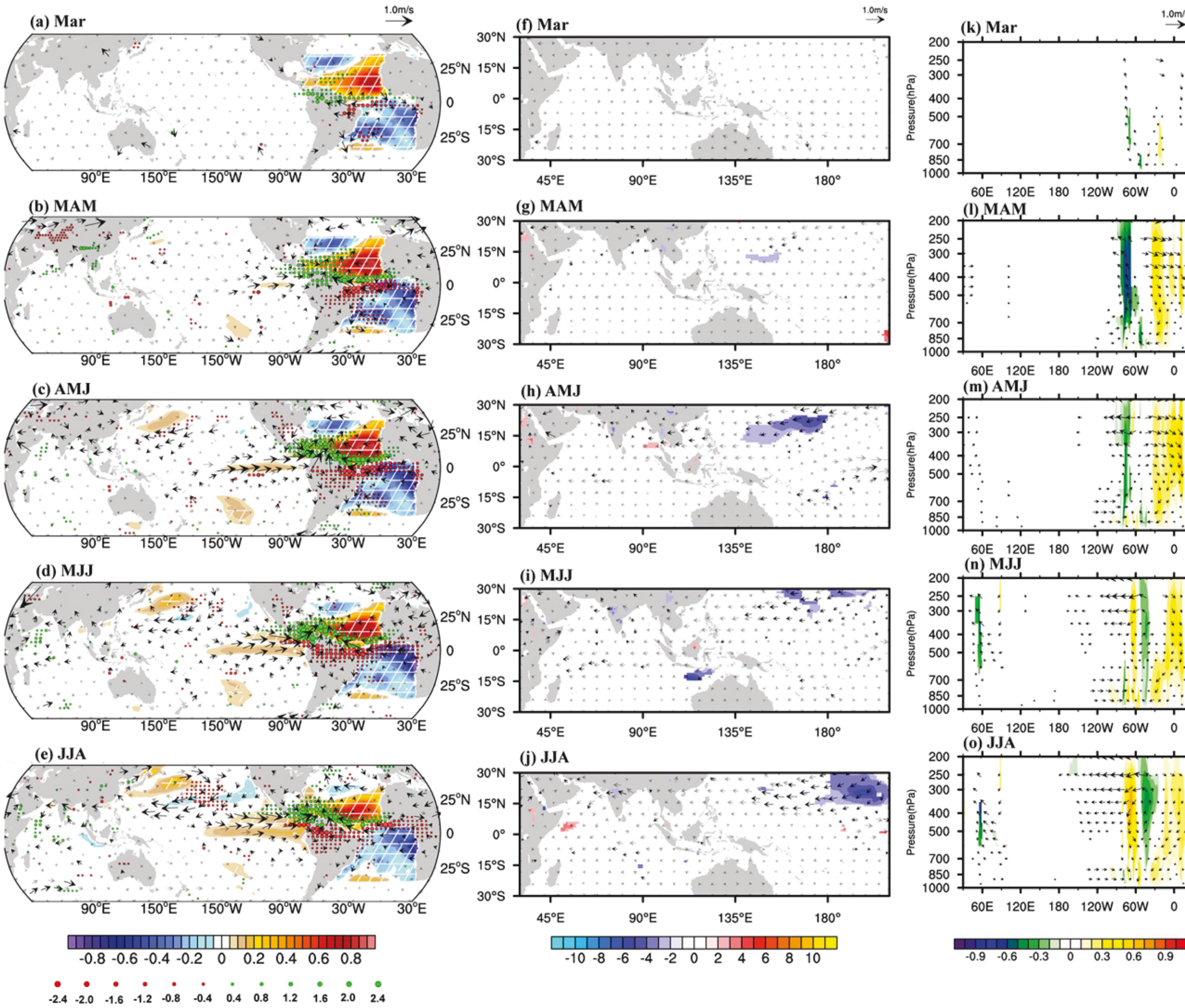

FIG. 6. As in Fig. 5, but for the results of EXP_EOF2.

by inducing an anticyclonic Rossby wave to the west. Wu et al. (2017a,b) further suggested that the moist enthalpy advection mechanism can act to maintain the anticyclonic circulations. Meanwhile, the significant descending motion over the equatorial central Pacific associated with the anomalous Walker circulation begins to be established during AMJ (Fig. 5m), and this anomalous descending motion is gradually enhanced from MJJ to JJA (Figs. 5n,o) with the strengthening of the NIO/MC positive heating and the formation of the central Pacific negative SSTA (Fig. 3b).

In contrast, for the meridional dipole forcing, during JJA, the tropical Atlantic heating is still a dipole structure (Fig. 3e). In response to this JJA Atlantic dipole heating, similar to the observations (Fig. 2e), the Kelvin wave response to the east (Figs. 6a–e) and the Kelvin wave–monsoon interaction (Figs. 6f–j) over the NIO/MC are negligible. But it is interesting to notice that the cyclonic Rossby circulation over the subtropical northeastern Pacific (Fig. 3e) in response to the dipole heating is stronger than MAM due to strengthening of the positive heating as the northward shift of the Atlantic ITCZ. This cyclonic circulation is associated with negative SSTA and negative heating over the subtropical central North Pacific. However, the easterly anomaly generated by this negative heating is only maintained in the off-equatorial region and the easterly anomaly over the EWP is negligible (Fig. 3e), which shows similar feature as the observations (Fig. 2e). Due to the weak Kelvin wave response to the dipole heating, the anomalous Walker circulation over the Pacific is also not established (Figs. 6k–o) and the La Niña condition is not developed afterward (Fig. 3f).

To sum up, the observational and modeling studies above indicate that the Atlantic's impact on the Pacific is pattern dependent. A basinwide tropical Atlantic forcing leads to a marked Kelvin wave response and associated wind–evaporation–SST–convection feedback over the NIO/MC sector, which eventually causes pronounced easterly anomalies over the equatorial western Pacific, promoting a La Niña development in the Pacific. On the other hand, the dipole SSTA pattern in the tropical Atlantic has little impact on the

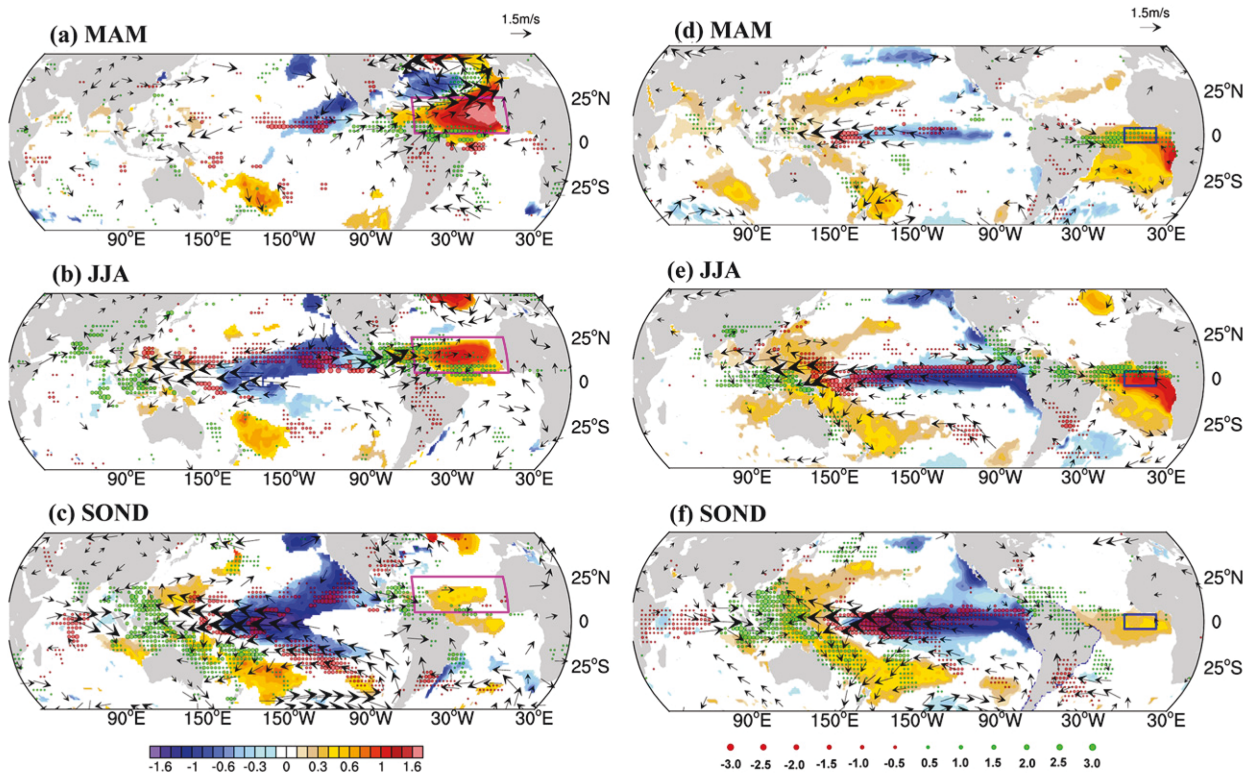

FIG. 7. Lagged partial-regression analysis of (a) MAM, (b) JJA, and (c) SOND SST (shading; °C), 850-hPa wind (vectors; m s^{-1}), and precipitation (dots; mm day^{-1}) on the MAM TNA index (5°–25°N, 70°–10°W, magenta box) during 1981–2018 with the effect of preceding JF Niño-3.4 index removed. (d)–(f) As in (a)–(c), but for regression on the EA index (4°S–4°N, 20°W–0°; blue box). Only the values above the 95% confidence level are plotted.

Indian and Pacific Oceans, due to the offsetting of the Kelvin wave to the Atlantic positive and negative heating. Both the Atlantic basin-warming and meridional dipole forcing could generate Rossby wave response to the west and the Rossby wave process can be coupled with the Kelvin wave process to contribute to the easterly anomaly over the EWP. However, when the Kelvin wave process is missing, the Rossby wave process alone for the meridional dipole forcing can only influence the zonal wind anomaly over the off-equatorial region, which cannot significantly influence the ENSO evolution. This suggests that the establishment of the Atlantic-induced Kelvin wave process is responsible for the significant (insignificant) impact of basin-warming (meridional dipole) forcing on ENSO evolution. Furthermore, the results above have important implications in real-time ENSO forecast. It is the pattern of the SSTA that matters, not an SSTA index in a certain region. A further discussion of this matter is given in section 5a.

4. Impacts of tropical North Atlantic and equatorial Atlantic SSTA on ENSO

In the previous section, we focus on examining the impacts of the tropical Atlantic basin-wide SSTA modes on the Pacific ENSO. In this section, we switch the focus to the widely used TNA and EA (or ATL3) indices. We would like to reexamine the physical mechanisms through which the TNA and EA SSTA modes affect the ENSO evolution and pattern diversity.

a. Observational analyses

The lagged partial-regression analysis is conducted to reveal the individual influence of the TNA and EA SSTA on the Pacific by regressing SSTA on the MAM TNA index and JJA EA index after removing the preceding wintertime Pacific ENSO impact (Fig. 7). The results show that a boreal spring TNA warming can induce a CP-type La Niña (Fig. 7c), whereas a boreal summer EA warming can induce an EP-type La Niña (Fig. 7f). The detailed discussion of the cause of the ENSO pattern diversity in response to the TNA and EA SSTA forcing will be shown in section 4c.

Previous studies suggested that the TNA-induced Rossby wave process over the subtropical northeastern Pacific (Ham et al. 2013a) and the EA-induced Walker circulation (Ding et al. 2012; Polo et al. 2015) are important in inducing the easterly anomaly over the equatorial western Pacific (Figs. 7a,d) to trigger La Niña events afterward. However, due to the limitation of the partial-regression analysis, it remains uncertain whether these mechanisms are entirely

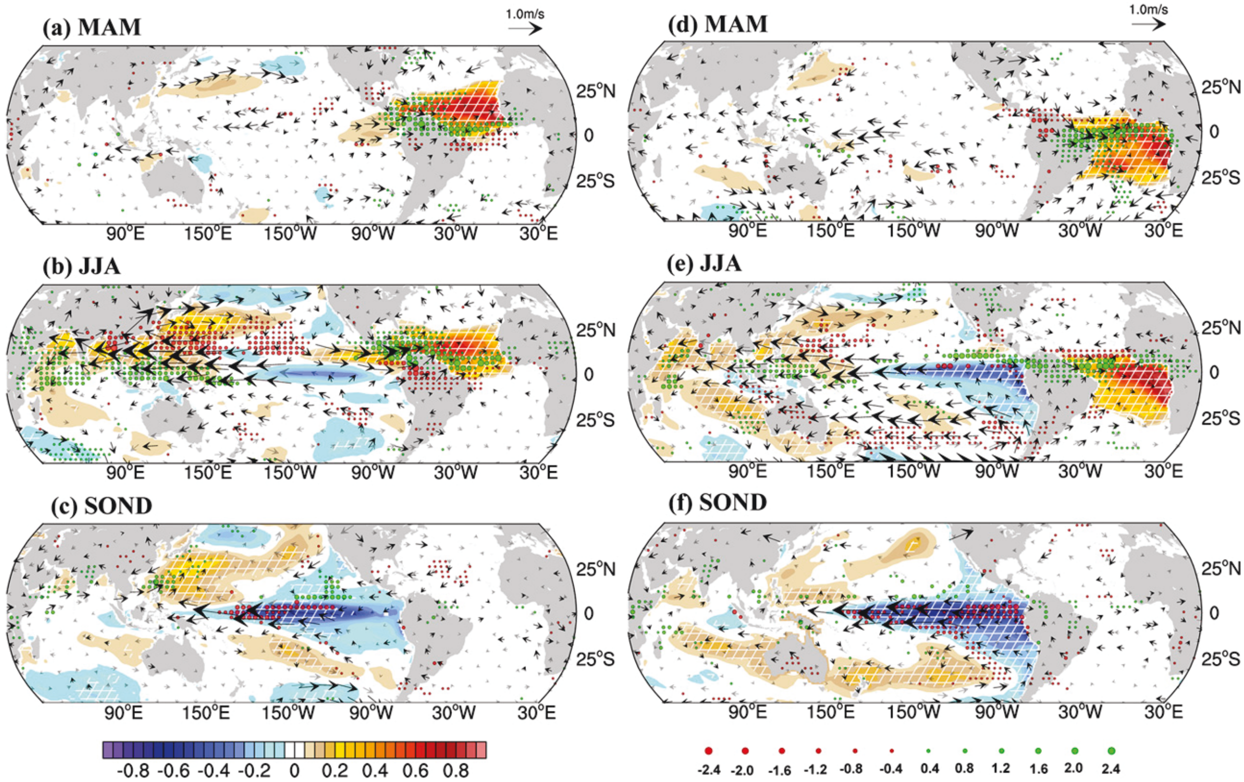

FIG. 8. Spatial evolution of model simulated SST (shading; °C), 850-hPa wind (vectors; m s^{-1}), and precipitation (dots; mm day^{-1}) for the EXP_TNA during (a) MAM, (b) JJA, and (c) SOND. (d)–(f) As in (a)–(c), but for the EXP_EA. The white hatched area, dotted area, and black vectors indicate values above the 95% confidence level.

driven by the Atlantic forcing. It is shown that during MAM, a significant cold SSTA signal already occurs over the subtropical northeastern Pacific (equatorial central Pacific) for the TNA (EA) regression (Figs. 7a,d) and these cold SSTA signals could be driven either by the Atlantic forcing or the preceding Pacific forcing. It is also uncertain whether the subtropical northeastern Pacific (equatorial central Pacific) SSTA in MAM is critical in generating the subsequent CP-type (EP-type) ENSO for TNA (EA) forcing. A detailed discussion of the relative roles of the initial Pacific SSTA pattern and the remote Atlantic forcing in determining the ENSO pattern diversity will be given in section 5b.

Moreover, our discussion from the previous section points out that the Atlantic-induced Kelvin wave process is important in conveying the impact from the Atlantic to the Pacific through interaction with the monsoonal circulation over the NIO/MC. As shown in Figs. 7b and 7e, significant positive rainfall anomaly occurs over the NIO/MC, which could further induce an easterly anomaly over the EWP. These positive rainfall anomalies might be partly induced by local warm SSTA that arises from the interaction between the easterly Kelvin wave and mean westerly monsoonal circulation. However, the positive SSTA over the northern Indian Ocean (Figs. 7b,e) is moderate possibly because of the damping effect of the reduced shortwave radiation caused by enhanced convection or the deficiency of the partial-regression analysis.

To further discuss the role of the Kelvin wave process in conveying the impact from the TNA and EA SSTA to the Pacific, idealized coupled model experiments with prescribed composite TNA and EA SSTA forcing are conducted in the following subsection.

b. *Idealized coupled model simulations*

The ensemble-mean simulation of SST, precipitation, and 850-hPa winds for the EXP_TNA/EXP_EA experiment is shown in Fig. 8, and the time evolution of the simulated Niño-3.4 index for ensemble members is shown in Fig. S5. Very similar to the observations (Fig. 7), the TNA warming (Fig. 8a) can induce a CP-type La Niña (Fig. 8c) while the EA warming (Fig. 8d) induces an EP-type La Niña (Fig. 8f).

For TNA warming forcing, during MAM, the Atlantic positive heating generates a cyclonic Rossby wave circulation to the west over the subtropical northeastern Pacific (Fig. 8a) and the northeasterly over the western flank of the cyclonic circulation induces negative heating locally through atmospheric dry advection (Ham et al. 2013a). This negative heating further generates an anticyclonic Rossby wave response to the west but this easterly anomaly in the southern flank of the anticyclonic circulation is mainly confined to the off-equatorial western Pacific region. Different from the observations, the cold SSTA generated by the Rossby wave is negligible and a discussion of the discrepancy between the observations and

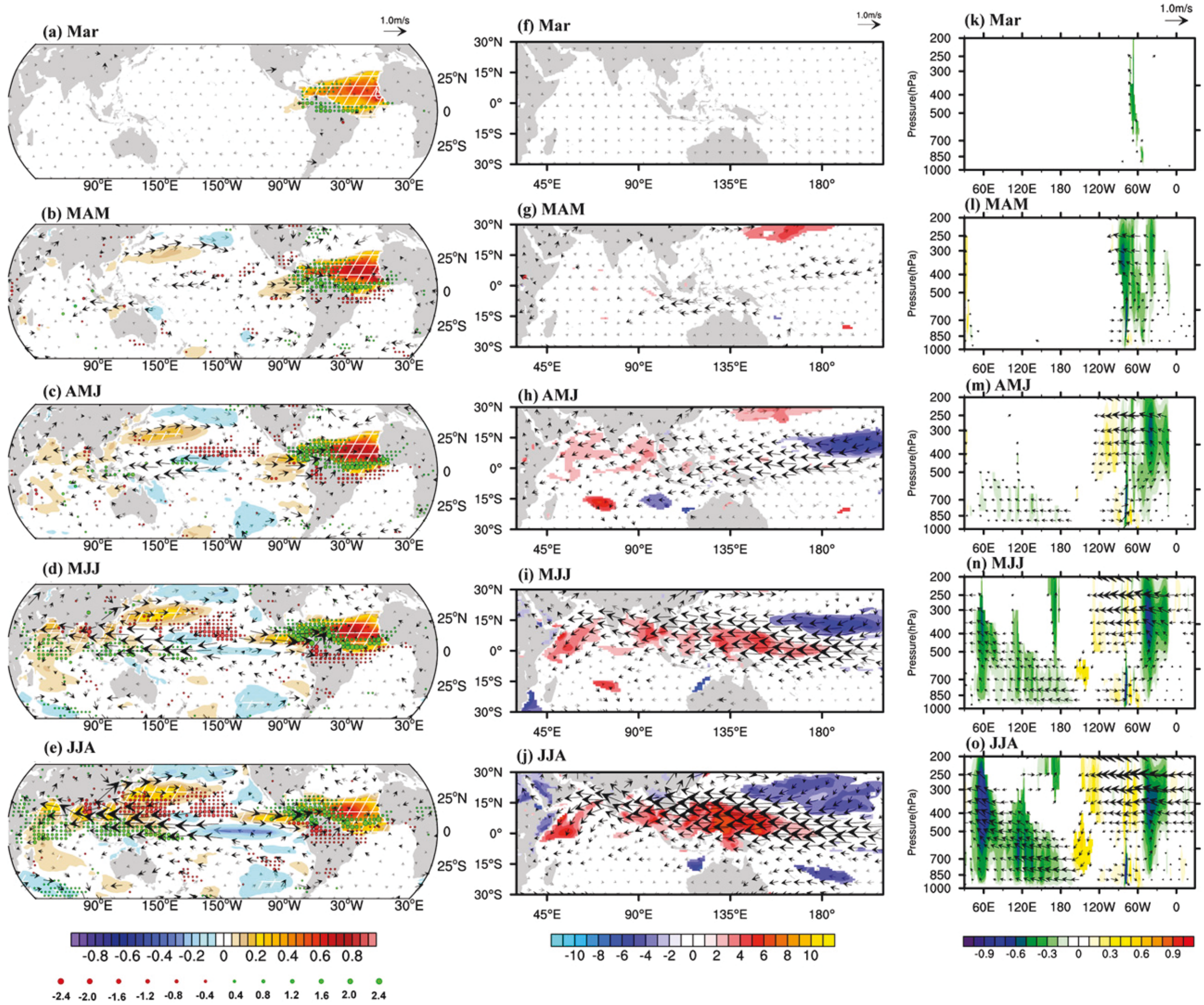

FIG. 9. As in Fig. 5, but for the results of EXP_TNA.

model simulations will appear in section 5. To the east, the Kelvin wave response is weak due to the presented dipole heating over the tropical Atlantic and the negative heating belt to the south is a result of the temperature gradient in the tropical Atlantic ITCZ region associated with the northward cross-equatorial flow. The detailed time evolution shows that as the positive heating north of equator becomes stronger, the easterly Kelvin wave over the Indian Ocean becomes significant and the SSTA warming associated with the positive rainfall anomaly occur over the NIO/MC from AMJ to JJA (Figs. 9c–e), which are also induced by the Kelvin wave–monsoon interaction through the wind–evaporation–SST–convection (WESC) feedback (Figs. 9h–j). This NIO/MC positive heating could further generate easterly anomalies over the EWP. Meanwhile, it is noted that the off-equatorial negative heating over the central North Pacific is also strengthened from AMJ to JJA (Figs. 9c–e) as the strengthening of the TNA-induced Rossby wave response and the Kelvin wave–induced anticyclonic shear. This negative heating also plays a role in enhancing the easterly anomaly over the EWP. As the easterly anomaly becomes significant over the EWP, the descending anomalies associated with the anomalous Walker circulation begins to be established (Fig. 9n) and the anomalous descent over the central Pacific is gradually enhanced from MJJ to JJA (Figs. 9n,o). Therefore, the significant easterly anomaly triggers La Niña event in subsequent fall and winter (Fig. 8c).

For EA warming forcing, during MAM, the equatorial Atlantic positive heating is mostly constrained in the central Atlantic (Fig. 8d), so the cyclonic Rossby wave response cannot extend far to the subtropical northeastern Pacific compared with the TNA forcing (Fig. 8a). To the east, the easterly Kelvin wave response extends from the tropical Indian Ocean to the western Pacific (Fig. 8d) and the easterly anomaly over the EWP is amplified by the warm SSTA and positive heating near the eastern Maritime Continent (Fig. 8d) that is induced by the increased latent heat flux (Fig. 10g) and the topographic lifting effect. This equatorial easterly anomaly begins to

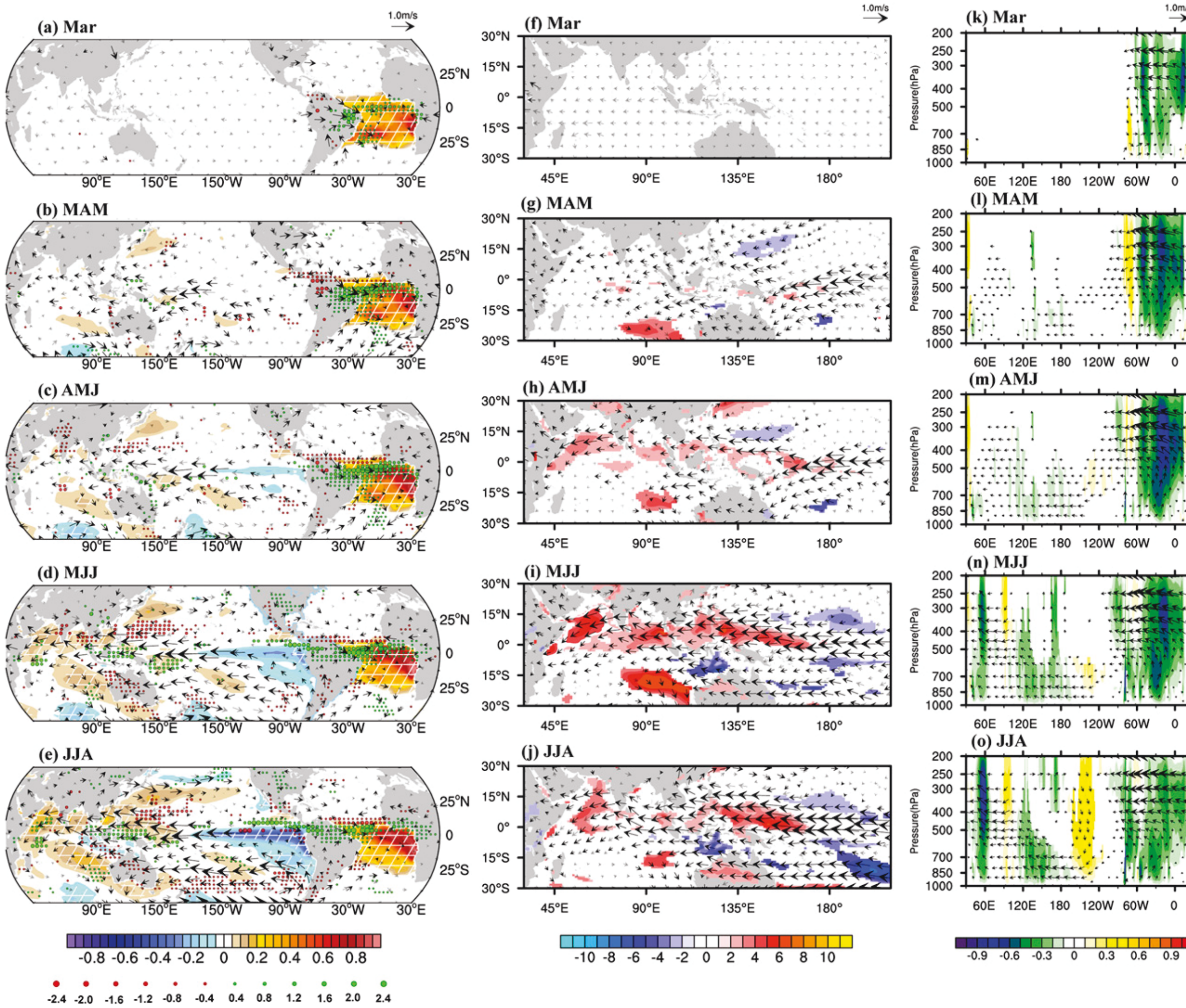

FIG. 10. As in Fig. 5, but for the results of EXP_EA.

generate upwelling Kelvin wave propagating eastward to influence the SSTA over the central-eastern Pacific and is gradually enhanced from AMJ to JJA (Figs. 10c–e) as the establishment of the warm SSTA and positive rainfall anomaly over the NIO/MC. Similar to the basin-warming forcing and the TNA forcing results, the warm SSTA and positive heating over the NIO/MC are also generated by the WESC feedback (Figs. 10h–j). The zonal circulation evolution (Figs. 10k–o) reveals that the descending anomaly over the central Pacific is weak from MAM (Fig. 10l) to May–July (MJJ; Fig. 10n) and the anomalous Walker circulation is well established during JJA (Fig. 10k). Previous studies (Ding et al. 2012; Polo et al. 2015) pointed out that the easterly anomaly over the EWP is generated by the anomalous divergence and descent over the central Pacific associated with a direct anomalous Walker circulation to the west of the Atlantic heat source. Here, our idealized numerical experiment with prescribed composite EA SSTA forcing indicates that the descent anomalies over the central Pacific is very weak from MAM to MJJ and is not sufficient to alter the convection over the central Pacific to generate the easterly anomaly over the EWP. Instead, our results suggest that the easterly anomaly over the EWP is part of the Kelvin wave response to the east of the Atlantic heat source and is amplified through the Kelvin wave–monsoon interaction and the associated WESC feedback over the NIO/MC sector. These processes eventually lead to the development of the cold SSTA over the central-eastern Pacific, the occurrence of anomalous descent over the equatorial central Pacific and the establishment of the anomalous Walker circulation.

Therefore, our numerical simulations demonstrate that for TNA forcing, both the Atlantic-induced Rossby wave process and Kelvin wave process can contribute to the easterly anomaly over equatorial western Pacific to influence the ENSO evolution. While for EA forcing, the Kelvin wave response and the associated WESC feedback over the NIO/MC plays a crucial role in influencing the easterly anomaly over the EWP. Also, the descent anomalies over the equatorial central Pacific for EA forcing do not result from a direct Walker

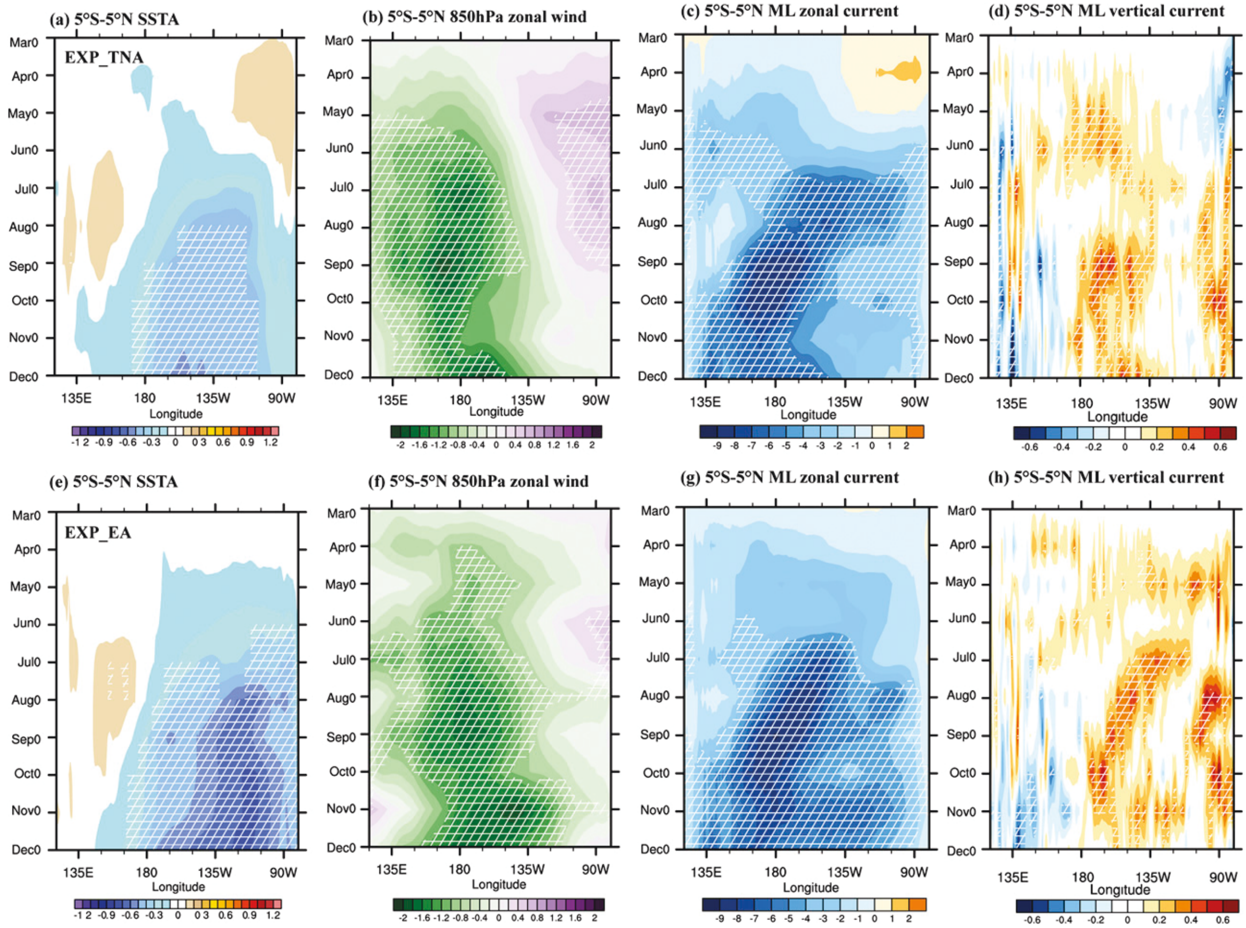

FIG. 11. Hovmöller diagram of 5°S–5°N averaged (a) SSTA, (b) 850-hPa zonal wind anomaly, (c) mixed layer averaged zonal current, and (d) mixed layer averaged vertical current for the EXP_TNA experiment. (e)–(h) As in (a)–(d), but for the EXP_EA experiment.

circulation response to the west of the EA forcing. Moreover, by comparing the simulation results of the TNA forcing (Figs. 8a–c),EA forcing (Figs. 8d,e), basin-warming forcing (Figs. 3a–c) and meridional dipole forcing (Figs. 3d–f), it is noticed that the Rossby wave process could be coupled with the Kelvin wave process to influence the zonal wind anomaly over the EWP (Figs. 8a–c and 3a–c) but if the Kelvin wave response is absent, the zonal wind anomaly over the EWP cannot be established (Figs. 3d–f), which suggests that the establishment of the Kelvin wave is essential in conveying the impact from the Atlantic to the Pacific.

c. ENSO pattern diversity in response to TNA and EA SSTA forcing

As mentioned in the previous study, the different responses of TNA and EA SSTA forcing can contribute to the diversity of ENSO patterns (Ham et al. 2013b). According to the observational analysis (Fig. 7) and the idealized model simulations (Fig. 8), our results also suggest that the TNA forcing tends to induce a CP-type ENSO, while the EA forcing prefers to generate an EP-type ENSO in subsequent winter. Ham et al. (2013b) pointed out that a stronger (weaker) zonal wind anomaly response to the TNA (EA) forcing over the equatorial eastern Pacific (EEP) might influence the oceanic vertical advection to contribute to the formation of the different types of ENSO. However, their argument was based on qualitative analysis only and the cause of the distinct zonal wind response over the EEP for TNA and EA forcing has not been clarified. In this subsection, we show a detailed evolution of the atmospheric and oceanic variables and conduct a mixed layer heat budget analysis following Chen et al. (2016), to further understand the key processes responsible for the different ENSO types.

The Hovmöller diagram of equatorial SSTA (Fig. 11) show that the significant SSTA signal for TNA forcing is mainly confined in the central Pacific (west of 135°W; Fig. 11a); however, the maximum SSTA signal for EA forcing occurs in the eastern Pacific (east of 135°W; Fig. 11e). It is worth noting that a SSTA warming appears over the EEP during March to June for TNA forcing, but a SSTA cooling develops in the EEP during boreal spring for EA forcing. The mixed layer temperature tendency anomaly evolution (Figs. 12a,e) also suggest that a general cooling tendency prevails over the central-eastern Pacific for both TNA and EA forcing during boreal summer and autumn. However, there is a significant difference

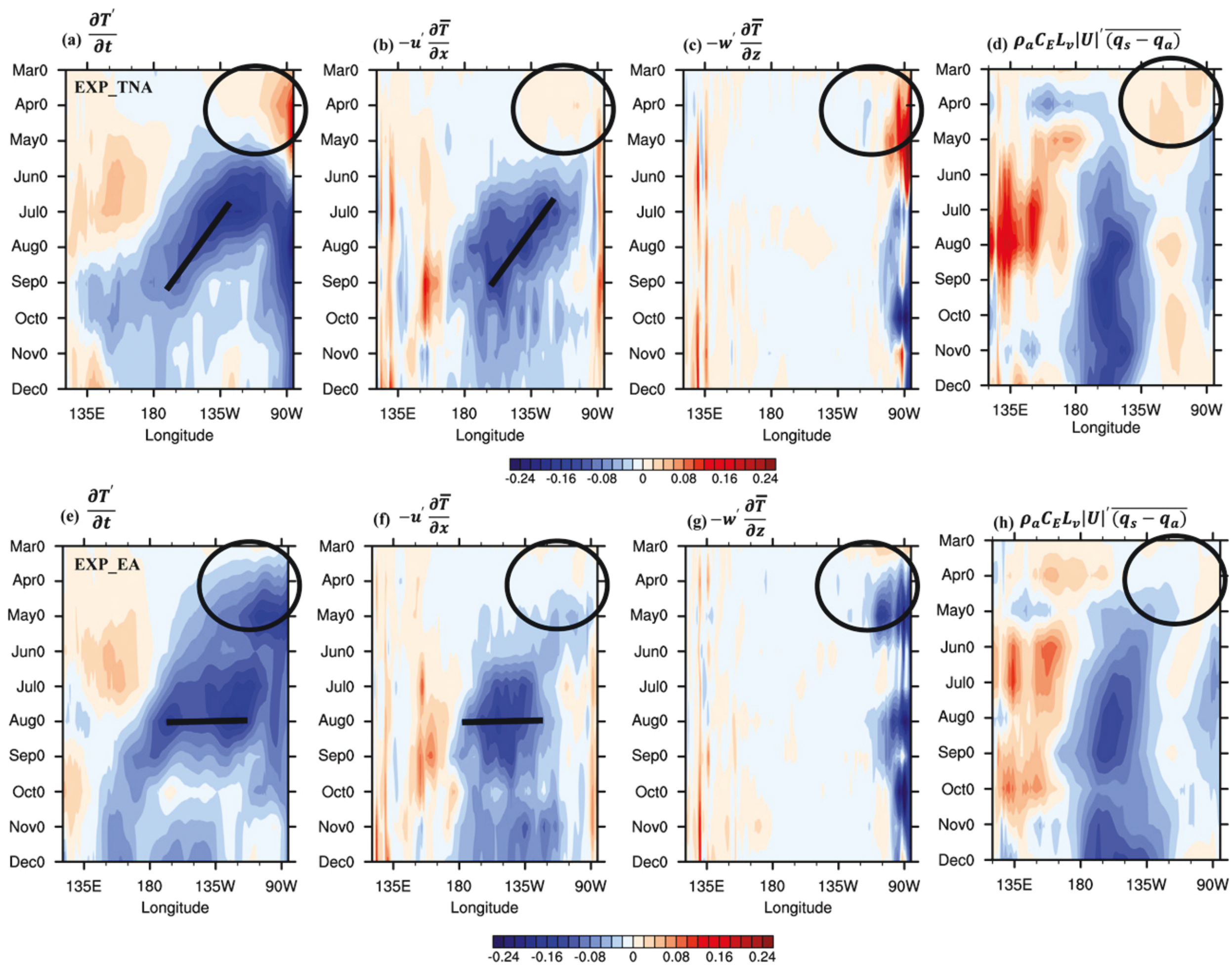

FIG. 12. Hovmöller diagram of 5°S–5°N averaged (a) mixed layer temperature anomaly tendency ($\partial T'/\partial t$), (b) anomalous zonal advection ($-u'\partial\overline{T}/\partial x$), (c) anomalous vertical advection ($-w'\partial\overline{T}/\partial z$), and (d) wind-induced latent heat flux anomaly [$\rho_a C_E L_v |U|'\overline{(q_s - q_a)}$] for the EXP_TNA experiment. (e)–(h) As in (a)–(d), but for the EXP_EA experiment.

between the TNA and EA forcing during the springtime (MAM). In the TNA forcing, the SSTA tended to warm over the eastern Pacific, whereas in the EA forcing the SSTA tended to cool over the eastern Pacific. This difference would directly cause the SSTA over the EEP for EA forcing to continuously develop from spring to winter and produce the maximum cooling SSTA in the eastern Pacific; in contrast, the cooling SSTA over the EEP for TNA forcing only begins to develop in summer, resulting in a stronger cooling SSTA in the central Pacific than in the eastern Pacific. Next, we will further investigate the reasons for the difference in EEP SSTA between TNA and EA forcing in spring according to the mixed layer heat budget analysis (see Figs. S6 and S7 for all the budget terms; here we only show the dominant terms related to the surface wind anomaly).

During MAM, a westerly anomaly over the EEP for TNA forcing (Fig. 11b) would generate eastward zonal current anomalies (Fig. 11c) to induce anomalous positive zonal advection (Fig. 12b; $-u'\partial\overline{T}/\partial x$). In the meantime, the downward vertical current anomalies appear over the EEP (Fig. 11d) according to the Ekman convergence, which induces positive vertical advection (Fig. 12c; $-w'\partial\overline{T}/\partial z$). The westerly anomaly also tends to reduce the climatological easterly wind to cause positive wind-induced latent heat flux component (Fig. 12d; see Fig. S8 for the linearization of latent heat flux). In contrast, for EA forcing, the westerly anomaly is absent over the EEP during MAM and the occupation of weak easterly anomaly results in westward zonal current (Fig. 11g) and anomalous upwelling over the EEP (Fig. 11h), which induce negative zonal advection (Fig. 12f) and vertical advection (Fig. 12g) to contribute to the cooling over the EEP during MAM. The wind-induced latent heat flux (Fig. 12h) over the EEP for EA forcing is also much weak than for the TNA forcing.

After springtime, for TNA forcing, even the zonal surface wind is still westerly anomaly during JJA over the EEP, the mixed layer zonal current turns westward (Fig. 11c) and is mainly dominated by the geostrophic current with the establishment of the zonal thermocline tilt, which has been previously diagnosed in Su et al. (2010). The westward current leads to upwelling over the EEP (Fig. 11d), which tends to contribute to the negative SSTA tendency over the EEP after springtime via generating negative zonal advection (Fig. 12b) and vertical advection (Fig. 12c). Moreover, it is noted that the maximum cold SSTA tendency (Fig. 12a) gradually shifts from eastern to central Pacific from June to September (black line in Fig. 12a), associated with the shifting of the zonal current (Fig. 11c) and the anomalous zonal advection (Fig. 12b). The relative stronger (weaker) cold SSTA tendency over the 180°–140°W (140°–100°W) during August–September could directly lead to the stronger (weaker) SSTA response during the wintertime, resulting in a CP-type response for TNA forcing. It is found that the occurrence of the westerly anomaly over the EEP from July to September (Fig. 11b) is responsible for the westward shift of the cold SSTA tendency. On one hand, the westerly anomaly could contribute to the Ekman current to weaken the total westward current to reduce the efficiency of the negative zonal advection (Fig. 12b) and on the other hand, the westerly anomaly could generate positive wind-induced latent heat flux (Fig. 12d) to reduce the cold SSTA tendency over 140°–100°W. Therefore, due to the late development of the cold SSTA over the EEP and the westward shift of the cold SSTA tendency, the TNA forcing finally generates a CP-type ENSO.

In contrast, for EA forcing, after springtime, due to the weak westerly anomaly over the EEP, the cold SSTA tendency does not show a westward shift feature (black line in Fig. 12e) and the cold SSTA continues to develop over the central-eastern Pacific through negative zonal advection and vertical advection. However, as the cold SSTA develops earlier over the EEP starting from MAM, the EA forcing finally results in an EP-type ENSO.

In conclusion, we believe the occupation of the surface westerly anomaly over the equatorial eastern Pacific holds a key in determining the ENSO type in the following winter. For TNA forcing, the significant westerly anomaly appears over the equatorial eastern Pacific during springtime and provides a warming SSTA tendency contributed by the anomalous warm zonal advection, anomalous warm vertical advection and wind induced evaporation effect, leading to the EEP cooling SSTA only begins to appear in summer. During summertime, the westerly anomaly also tends to shift the maximum cold SSTA tendency westward through reducing the westward zonal current and evaporation over the EEP. The late development of the cold SSTA over the EEP and the westward shift of the cold SSTA tendency results in a CP-type ENSO for TNA forcing. For EA forcing, the absence of the westerly anomaly cannot generate warming over the EEP during springtime and the EEP cooling SSTA can continuously develop from spring to winter and generate an EP-type ENSO.

The difference in the equatorial wind response over the EEP is likely a result of longitudinal locations of anomalous heat source associated with the TNA and EA SSTA modes. The TNA heating can extend to the western Atlantic warm pool (Fig. 8a), whereas the EA heating is mostly confined to the central Atlantic ITCZ region (Fig. 8d). As a result, the Rossby wave response to the TNA heating can extend farther westward compared to that of the EA forcing. This explains the much stronger wind response over the far equatorial eastern Pacific in the TNA forcing scenario.

5. Discussion

a. A cautious note on real-time ENSO forecast with the TNA and EA indices

Although the results above point out the distinctive impacts of the TNA and EA SSTA indices on the ENSO type, a caution is needed in real-time prediction using the indices. Note that the regression patterns in Fig. 7 show rather ''clean'' SSTA structures in the tropical Atlantic. For instance, for the TNA regression, a marked warm SSTA appears in boreal spring, while the SSTA in the equatorial Atlantic is near zero. The similar feature is seen in the EA regression. Because of the clean SSTA pattern, the TNA and EA impacts on the Pacific are clearly presented (Figs. 7 and 8). On the other hand, the results from section 3 show that the impacts of the tropical Atlantic basin-warming and dipole SSTA patterns on ENSO are quite different. The former is able to trigger a strong Kelvin wave and Kelvin wave–monsoon interaction over the NIO/MC, whereas the latter cannot. This indicates that considering the tropical Atlantic SSTA as precursors for ENSO, the SSTA pattern is more important. When the TNA and EA forcing are presented with the same sign, the Atlantic's influence on the Pacific would be more robust. When they are in an opposite sign, the impact of the Atlantic to the Pacific could be much weaker due to the offsetting effect of the dipole heating.

To reveal the observed characteristics of the SSTA pattern associated with the individual TNA and EA SSTA events, we calculated the area-averaged SSTA values in both the TNA and EA regions for each of the significant TNA and EA warming/cooling cases. All TNA (EA) cases with its index in MAM (JJA) exceeds 0.8 standard deviations are selected. Figures 13a and 13b show all these TNA cases. Note that about a half of these TNA cases are accompanied by the same sign of the equatorial Atlantic SSTA condition, whereas another half are accompanied with an opposite sign (Figs. 13a,b). A similar situation happens for the selected EA cases (Figs. 13c,d). Thus, one needs to pay special attention to the pattern of the tropical Atlantic SSTA rather than just the TNA or EA index.

b. Relative roles of the initial Pacific SSTA pattern versus the remote Atlantic forcing in determining the ENSO pattern diversity

The observational analysis and idealized CGCM simulation in section 4 show that the TNA (EA) warming can induce a CP-type (EP-type) La Niña, which is mainly attributed to a westerly (easterly) anomaly over the equatorial eastern Pacific that is caused by the strong (weak) Rossby wave response to the Atlantic forcing. However, an obvious discrepancy between the observational analysis (Fig. 7) and model simulation (Fig. 8) is that for the observational analysis, during MAM, a significant cold SSTA signal already occurs over the

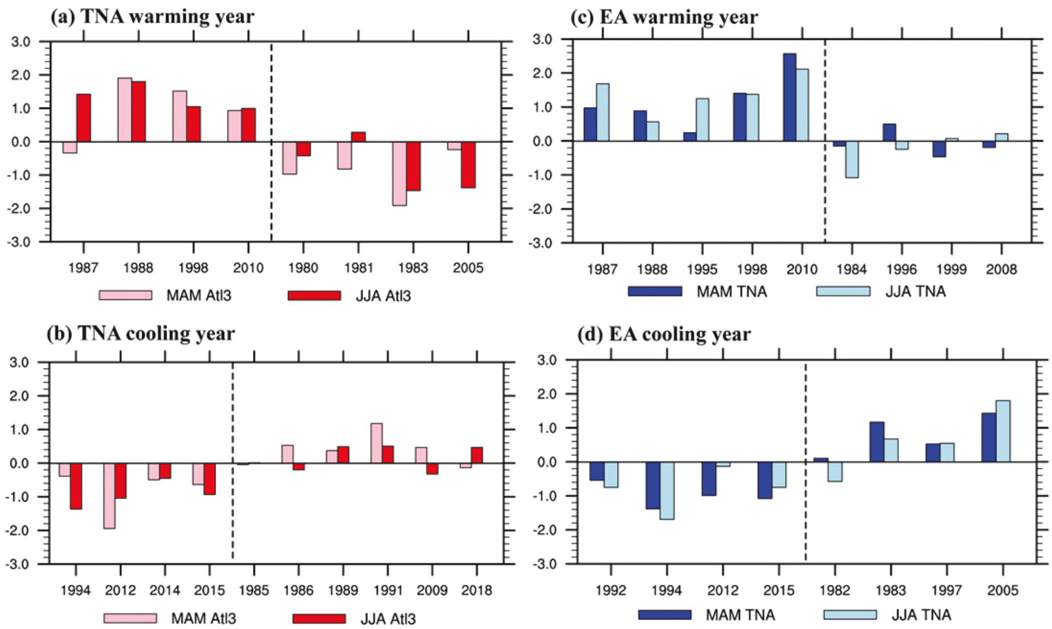

FIG. 13. (a) MAM EA index (pink bar) and JJA EA index (red bar) for TNA warming cases. (b) As in (a), but for TNA cooling cases. (c) MAM TNA index (blue bar) and JJA TNA index (light blue bar) for EA warming cases. (d) As in (c), but for EA cooling cases. All TNA (EA) cases are selected with an index in MAM (JJA) exceeding 0.8 standard deviation.

subtropical northeastern Pacific (equatorial central Pacific) for the TNA (EA) forcing, even though a partial regression analysis has been applied to remove the preceding boreal winter SSTA signal in the tropical Pacific. For the model simulation, the Pacific SSTA signal in MAM is negligible. Therefore, it is uncertain whether or not the subtropical northeastern Pacific (equatorial central Pacific) SSTA in MAM is critical in generating the subsequent CP-type (EP-type) ENSO response.

To investigate the initial Pacific SSTA condition on the subsequent ENSO evolution, we conduct two additional sets of sensitivity experiments in which we remove the Atlantic SSTA forcing but keep the initial MAM Pacific SSTA shown in Fig. 7. The control experiment (EXP_PAC_CTRL) denotes that the tropical Pacific is prescribed with climatological SST during MAM, whereas other regions are freely coupled. The configuration for the sensitivity experiment (EXP_PACini_TNA) is the same as the control experiment except that the MAM subtropical northeastern Pacific cold SSTA that is obtained from the partial-regression analysis (Fig. 7a) is added on the climatological SST.

It is shown from Figs. 14a–c that the MAM subtropical Pacific cold SSTA could generate an easterly anomaly in the equatorial western Pacific, and thereby a La Niña in subsequent winter, but as the westerly anomaly response over the eastern Pacific is weak, the CP-type La Niña is not obvious (Fig. 14c). A similar experiment (EXP_PACini_EA) is also applied for the EA warming case, in which the MAM equatorial Pacific cold SSTA (Fig. 7d) is prescribed. The results show that the equatorial Pacific initial cold SSTA could induce an EP-type La Niña in subsequent winter (Fig. 14f) due to the weak westerly over the eastern Pacific. Therefore, it is shown that given the Pacific MAM initial SSTA (Figs. 7a,d) only, the ENSO type cannot be clearly clarified (Fig. 14). When TNA and EA forcing are prescribed, the CP-type and EP-type ENSO can be simulated more clearly (Fig. 8), which indicates that the Atlantic forcing is critical in contributing to ENSO pattern diversity. However, caution is needed that the existence of the TNA forcing cannot guarantee the occurrence of the CP-type ENSO, although it can modulate the ENSO type.

The current modeling experiments examine the influence of different tropical Atlantic forcing on the Pacific, including the Atlantic basin-warming forcing, meridional dipole forcing, tropical North Atlantic forcing, and equatorial Atlantic forcing. By comparing the simulation results of these four sets of experiments (Figs. 3 and 5), it is revealed that the Rossby wave process could be coupled with the Kelvin wave process to influence the zonal wind anomaly over the equatorial western Pacific. However, if the Kelvin wave response is absent, the zonal wind anomaly over the equatorial western Pacific and the subsequent ENSO condition cannot be established, indicating the essential role of the Kelvin wave process in conveying the impact from the Atlantic to the Pacific. However, even though the model can simulate the Rossby wave response and the atmospheric advection process associated with the Rossby wave circulation, the air–sea interaction process generated by the Rossby wave circulation is weaker in simulations than in observations, especially during MAM. This discrepancy might be attributed to the following three hypotheses. First, as the SSTA forcing magnitude over the tropical Atlantic is moderate, the

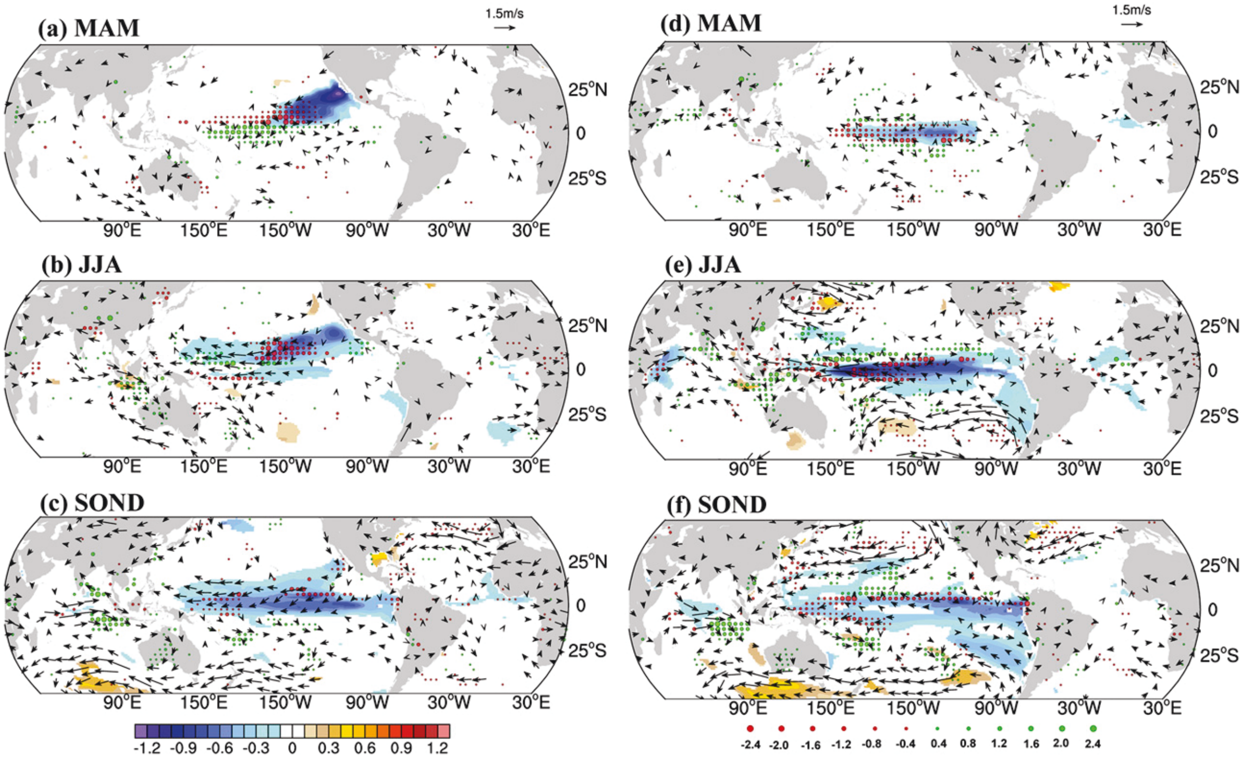

FIG. 14. Spatial evolution of model simulated SST (shading; °C), 850-hPa wind (vectors; m s^{-1}), and precipitation (dots; mm day^{-1}) for the EXP_PACini_TNA minus EXP_PAC_CTRL during (a) MAM, (b) JJA, and (c) SOND. (d)–(f) As in (a)–(c), but for the difference between EXP_PACini_EA and EXP_PAC_CTRL. Only the values above the 90% confidence level are plotted.

Atlantic forcing alone in the model may not be sufficient to generate significant air–sea interaction over the subtropical northeastern Pacific. One previous study (Ham et al. 2013a) successfully simulated the air–sea interaction over the subtropical northeastern Pacific during JJA with a stronger TNA forcing but the air–sea interaction during MAM is also negligible (their Fig. S4). Second, it is also possible that the model tends to underestimate the Rossby wave induced air–sea interaction due to the model bias problem and our results could also be model dependent. Third, the strong Rossby wave–induced air–sea interaction in observations might be due to the preceding ENSO influence is not completely removed by partial-regression analysis and the strong signals may not be purely generated by the Atlantic forcing. A future study is needed to investigate the possible reasons for the discrepancies of the Rossby wave–induced air–sea interaction process in the subtropical northeastern Pacific between the observations and model simulation. Composite analysis of the Atlantic SSTA events with or without ENSO condition in preceding winter toward the CMIP model outputs might give us some clues.

6. Conclusions

In this study, the impacts of the TNA and EA SSTA on ENSO are investigated through observational analyses and numerical simulations. First, the impact of the basinwide SSTA modes in the tropical Atlantic on ENSO is examined. An EOF analysis of the spring–summer SSTA over the tropical Atlantic shows two dominant modes: a basin-warming mode and a meridional dipole mode. For the observational analysis, the impacts of the basin-warming forcing and north–south dipole forcing on the Pacific are investigated through a lagged partial-regression analysis with respect to the normalized PC-1 and PC-2 after excluding the preceding ENSO effect. As the partial-regression analysis cannot completely eliminate the preceding ENSO signal due to the different ENSO temporal evolution and the small sample size, the idealized partially coupled model experiments with prescribed Atlantic forcing are further conducted to examine the pure impact of the basin-warming forcing and dipole forcing on the Pacific. Both the observational analyses and model simulation show clearly that the basin-warming forcing leads to a La Niña in the subsequent winter while the meridional dipole forcing cannot.

It is found that both basin-warming forcing and meridional dipole forcing can generate the Rossby wave response over the subtropical northeastern Pacific, but the easterly anomaly over the equatorial western Pacific (EWP) is only significant for the basin-warming forcing; it is negligible for the dipole forcing. This easterly anomaly over the EWP is essential for triggering La Niña event by inducing upwelling Kelvin wave propagating eastward. Our numerical experiments indicate that the significant (insignificant) wind response over the EWP is mainly attributed to the strong (negligible) Kelvin wave response to the basin-warming (meridional dipole) forcing. For the basin-

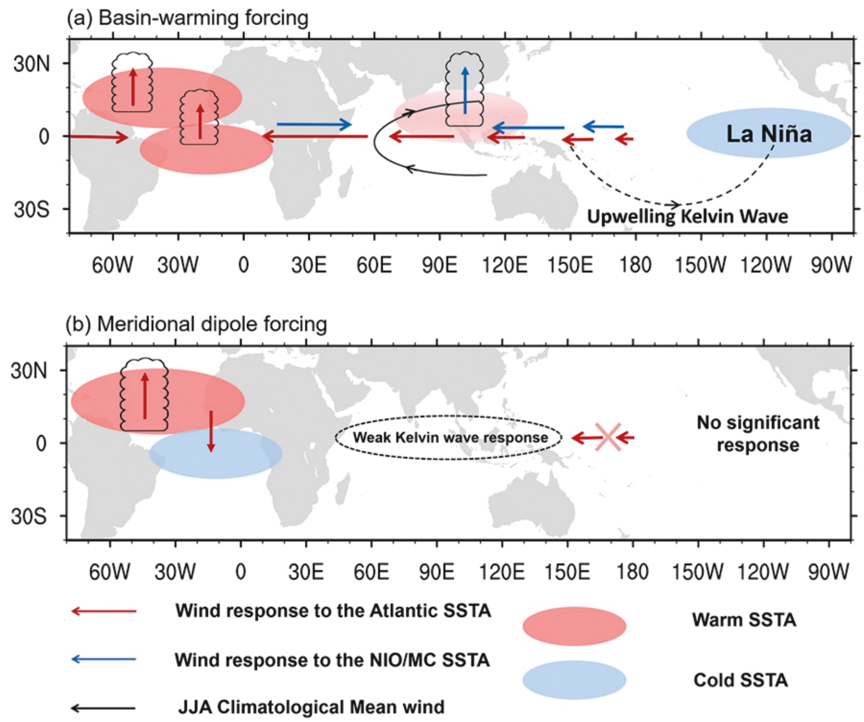

FIG. 15. Schematic diagram for how the (a) basin-warming forcing and (b) meridional dipole forcing influences the Pacific through Kelvin wave–monsoon interaction over the northern Indian Ocean (NIO) and Maritime Continent (MC). Red (blue) shading denotes the SSTA warming (cooling); red vectors indicate the wind response to the tropical Atlantic heating; blue vectors represent the wind response to the NIO/MC heating; black vectors represent the JJA climatological mean wind; a red cross sign over the equatorial western Pacific in (b) indicates the lack of an easterly anomaly.

warming forcing, the Atlantic heating induces a significant Kelvin wave easterly to the east, which interacts with the mean monsoonal westerly and causes warm SST and positive precipitation anomalies over the northern Indian Ocean (NIO)/Maritime Continent (MC) sector through a wind–evaporation–SSTA–convection (WESC) feedback. The model simulation results show clearly that the easterly anomaly induces increased surface latent heat flux (positive downward) in situ, accompanied by the formation of warm SST and positive heating anomalies over the NIO/MC (schematic diagram is shown in Fig. 15a). However, for the meridional dipole forcing, the Kelvin wave in response to the Atlantic dipole heating is much weaker due to the cancellation of the positive and negative heating effects in the Atlantic. As a result, the easterly anomaly over the EWP and the subsequent La Niña event are not significant (schematic diagram is shown in Fig. 15b).

Next, we examine the impacts of the TNA and EA SSTA on ENSO evolution and pattern diversity. The idealized coupled model experiments with prescribed composite SSTA forcing over the TNA and EA region indicate that the TNA (EA) forcing can generate a CP-type (EP-type) La Niña in the subsequent winter. Again, the Kelvin wave response and associated WESC feedback over the NIO/MC play important roles in influencing the easterly anomaly over the EWP in both the TNA and EA forcing scenarios. Previous studies (Ding et al. 2012; Polo et al. 2015) suggested that the easterly anomaly over the EWP for EA forcing is generated by the anomalous descent over the central Pacific associated with a direct EA-induced anomalous Walker circulation. Here, our numerical experiment with prescribed EA forcing indicates that the easterly anomaly over the EWP is part of the Kelvin wave response to the east of the Atlantic heat source and is amplified through the Kelvin wave–monsoon interaction over the NIO/MC sector. These processes eventually lead to the establishment of anomalous descent over the equatorial central Pacific, and we found that the EA-induced Walker circulation is not the primary cause for the easterly anomaly over the EWP but is the final equilibrium state during the summertime.

The cause of the distinctive CP- and EP-type ENSO between the TNA and EA forcing lies in the anomalous wind response mainly during MAM in the equatorial eastern Pacific. Because of the westward location of the TNA heating, a marked westerly anomaly response appears over the equatorial eastern Pacific. This is in contrast to the EA forcing, which shows a weak easterly response there. A mixed layer heat budget analysis shows that the surface westerly (easterly) wind stress anomaly is crucial in dissipating (promoting) the local cooling through anomalous zonal ($-u'\partial\overline{T}/\partial x$) and vertical

$(-w'\partial\overline{T}/\partial z)$ advection and wind-induced evaporation process $[\rho_a C_E L_v |U|'\overline{(q_a - q_s)}]$. All these processes above generate a warm (cold) SSTA tendency during MAM and lead to the late (early) growth of the cold SSTA over the equatorial eastern Pacific. As a result, the TNA forcing leads to the formation of a CP-type La Niña while the EA forcing favors the development of an EP-type La Niña.

In summary, from the different perspectives of the basinwide SSTA and TNA/EA SSTA forcing, we demonstrate the important role of the heating induced Kelvin wave response and the associated WESC feedback in conveying the Atlantic's impact to the Pacific. The distinctive impacts of the basinwide and the meridional dipole SSTA patterns on the Pacific warn us that a caution is needed in considering the tropical Atlantic SSTA as precursors for the ENSO forecast. Not only the amplitude but also the pattern of the SSTA in the tropical Atlantic matter. As to the TNA and EA indices, again not only the magnitude but also the relative sign of the TNA and EA indices are crucial. When the two indices are presented with the same sign, the Atlantic's influence on the Pacific would be more robust. When they are in an opposite sign, the impact of the Atlantic to the Pacific would be much weaker due to the offsetting of the Kelvin wave response. Thus, in the real-time forecast, one needs to pay special attention to the pattern of the tropical Atlantic SSTA rather than just the TNA or EA index.

Acknowledgments. The authors thank Dr. Bo Wu and Mr. Yu Huang for helping understand the CESM model code and set up sensitivity experiments. We would also like to acknowledge high-performance computing support from Cheyenne (https://doi.org/10.5065/D6RX99HX) provided by NCAR's Computational and Information Systems Laboratory, sponsored by the National Science Foundation. This work was supported by NSFC project 42088101, NSF AGS-2006553, and NOAANA18OAR4310282. This is SOEST contribution number 11350 and IPRC contribution number 1523.

Date availability statement. The Hadley SST dataset is available at https://www.metoffice.gov.uk/hadobs/hadisst/data/download.html. The NCEP–NCAR monthly reanalysis is available at https://psl.noaa.gov/data/gridded/data.ncep.reanalysis2.html. The GPCP dataset is available at http://www.esrl.noaa.gov/psd/. Any other data are available upon request from the corresponding author.

REFERENCES

Adler, R. F., and Coauthors, 2003: The version-2 Global Precipitation Climatology Project (GPCP) monthly precipitation analysis (1979–present). *J. Hydrometeor.*, **4**, 1147–1167, https://doi.org/10.1175/1525-7541(2003)004<1147:TVGPCP>2.0.CO;2.

Alexander, M., and J. Scott, 2002: The influence of ENSO on air–sea interaction in the Atlantic. *Geophys. Res. Lett.*, **29**, 1701, https://doi.org/10.1029/2001GL014347.

Cai, W., and Coauthors, 2019: Pantropical climate interactions. *Science*, **363**, eaav4236, https://doi.org/10.1126/science.aav4236.

Carton, J. A., and B. Huang, 1994: Warm events in the tropical Atlantic. *J. Phys. Oceanogr.*, **24**, 888–903, https://doi.org/10.1175/1520-0485(1994)024<0888:WEITTA>2.0.CO;2.

Chang, P., Y. Fang, R. Saravanan, L. Ji, and H. Seidel, 2006: The cause of the fragile relationship between the Pacific El Niño and the Atlantic Niño. *Nature*, **443**, 324–328, https://doi.org/10.1038/nature05053.

Chen, M., T. Li, X. Shen, and B. Wu, 2016: Relative roles of dynamic and thermodynamic processes in causing evolution asymmetry between El Niño and La Niña. *J. Climate*, **29**, 2201–2220, https://doi.org/10.1175/JCLI-D-15-0547.1.

Chiang, J. C. H., and A. H. Sobel, 2002: Tropical tropospheric temperature variations caused by ENSO and their influence on the remote tropical climate. *J. Climate*, **15**, 2616–2631, https://doi.org/10.1175/1520-0442(2002)015<2616:TTTVCB>2.0.CO;2.

Ding, H., N. S. Keenlyside, and M. Latif, 2012: Impact of the equatorial Atlantic on the El Niño Southern Oscillation. *Climate Dyn.*, **38**, 1965–1972, https://doi.org/10.1007/s00382-011-1097-y.

Enfield, D. B., and D. A. Mayer, 1997: Tropical Atlantic sea surface temperature variability and its relation to El Niño–Southern Oscillation. *J. Geophys. Res.*, **102**, 929–945, https://doi.org/10.1029/96JC03296.

Gill, A. E., 1980: Some simple solutions for heat-induced tropical circulation. *Quart. J. Roy. Meteor. Soc.*, **106**, 447–462, https://doi.org/10.1002/qj.49710644905.

Ham, Y.-G., and J.-S. Kug, 2015: Role of north tropical Atlantic SST on the ENSO simulated using CMIP3 and CMIP5 models. *Climate Dyn.*, **45**, 3103–3117, https://doi.org/10.1007/s00382-015-2527-z.

——, ——, J.-Y. Park, and F.-F. Jin, 2013a: Sea surface temperature in the north tropical Atlantic as a trigger for El Niño/Southern Oscillation events. *Nat. Geosci.*, **6**, 112–116, https://doi.org/10.1038/ngeo1686.

——, ——, and ——, 2013b: Two distinct roles of Atlantic SSTs in ENSO variability: North tropical Atlantic SST and Atlantic Niño. *Geophys. Res. Lett.*, **40**, 4012–4017, https://doi.org/10.1002/grl.50729.

Horel, J. D., and J. M. Wallace, 1981: Planetary-scale atmospheric phenomena associated with the Southern Oscillation. *Mon. Wea. Rev.*, **109**, 813–829, https://doi.org/10.1175/1520-0493(1981)109<0813:PSAPAW>2.0.CO;2.

Hurrell, J. W., and Coauthors, 2013: The Community Earth System Model: A framework for collaborative research. *Bull. Amer. Meteor. Soc.*, **94**, 1339–1360, https://doi.org/10.1175/BAMS-D-12-00121.1.

Jiang, L., and T. Li, 2019: Relative roles of El Niño-induced extratropical and tropical forcing in generating tropical North Atlantic (TNA) SST anomaly. *Climate Dyn.*, **53**, 3791–3804, https://doi.org/10.1007/s00382-019-04748-7.

Kanamitsu, M., W. Ebisuzaki, J. Woollen, S.-K. Yang, J. J. Hnilo, M. Fiorino, and G. L. Potter, 2002: NCEP–DOE AMIP-II Reanalysis (R-2). *Bull. Amer. Meteor. Soc.*, **83**, 1631–1644, https://doi.org/10.1175/BAMS-83-11-1631.

Keenlyside, N. S., and M. Latif, 2007: Understanding equatorial Atlantic interannual variability. *J. Climate*, **20**, 131–142, https://doi.org/10.1175/JCLI3992.1.

——, H. Ding, and M. Latif, 2013: Potential of equatorial Atlantic variability to enhance El Niño prediction. *Geophys. Res. Lett.*, **40**, 2278–2283, https://doi.org/10.1002/grl.50362.

Klein, S. A., B. J. Soden, and N.-C. Lau, 1999: Remote sea surface temperature variations during ENSO: Evidence for a tropical atmospheric bridge. *J. Climate*, **12**, 917–932, https://doi.org/10.1175/1520-0442(1999)012<0917:RSSTVD>2.0.CO;2.

Kosaka, Y., and S.-P. Xie, 2013: Recent global-warming hiatus tied to equatorial Pacific surface cooling. *Nature*, **501**, 403–407, https://doi.org/10.1038/nature12534.

Lee, S.-K., D. B. Enfield, and C. Wang, 2008: Why do some El Niños have no impact on tropical North Atlantic SST? *Geophys. Res. Lett.*, **35**, L16705, https://doi.org/10.1029/2008GL034734.

Li, T., and B. Wang, 1994: A thermodynamic equilibrium climate model for monthly mean surface winds and precipitation over the tropical Pacific. *J. Atmos. Sci.*, **51**, 1372–1385, https://doi.org/10.1175/1520-0469(1994)051<1372:ATECMF>2.0.CO;2.

——, ——, B. Wu, T. Zhou, C.-P. Chang, and R. Zhang, 2017: Theories on formation of an anomalous anticyclone in western North Pacific during El Niño: A review. *J. Meteor. Res.*, **31**, 987–1006, https://doi.org/10.1007/s13351-017-7147-6.

Lübbecke, J. F., and M. J. McPhaden, 2012: On the inconsistent relationship between Pacific and Atlantic Niños. *J. Climate*, **25**, 4294–4303, https://doi.org/10.1175/JCLI-D-11-00553.1.

——, B. Rodríguez-Fonseca, I. Richter, M. Martín-Rey, T. Losada, I. Polo, and N. S. Keenlyside, 2018: Equatorial Atlantic variability—Modes, mechanisms, and global teleconnections. *Wiley Interdiscip. Rev.: Climate Change*, **9**, e527, https://doi.org/10.1002/wcc.527.

Neale, R. B., J. Richter, S. Park, P. H. Lauritzen, S. J. Vavrus, P. J. Rasch, and M. Zhang, 2013: The mean climate of the Community Atmosphere Model (CAM4) in forced SST and fully coupled experiments. *J. Climate*, **26**, 5150–5168, https://doi.org/10.1175/JCLI-D-12-00236.1.

Park, J.-H., and T. Li, 2018: Interdecadal modulation of El Niño–tropical North Atlantic teleconnection by the Atlantic multidecadal oscillation. *Climate Dyn.*, **52**, 5345–5360, https://doi.org/10.1007/s00382-018-4452-4.

Philander, S. G. H., 1983: El Niño Southern Oscillation phenomena. *Nature*, **302**, 295–301, https://doi.org/10.1038/302295a0.

Polo, I., B. Rodríguez-Fonseca, T. Losada, and J. García-Serrano, 2008: Tropical Atlantic variability modes (1979–2002). Part I: Time-evolving SST modes related to West African rainfall. *J. Climate*, **21**, 6457–6475, https://doi.org/10.1175/2008JCLI2607.1.

——, M. Martin-Rey, B. Rodriguez-Fonseca, F. Kucharski, and C. R. Mechoso, 2015: Processes in the Pacific La Niña onset triggered by the Atlantic Niño. *Climate Dyn.*, **44**, 115–131, https://doi.org/10.1007/s00382-014-2354-7.

Rayner, N. A., D. E. Parker, E. B. Horton, C. K. Folland, L. V. Alexander, D. P. Rowell, E. C. Kent, and A. Kaplan, 2003: Global analyses of sea surface temperature, sea ice, and night marine air temperature since the late nineteenth century. *J. Geophys. Res.*, **108**, 4407, https://doi.org/10.1029/2002JD002670.

Richter, I., S.-P. Xie, A. T. Wittenberg, and Y. Masumoto, 2012: Tropical Atlantic biases and their relation to surface wind stress and terrestrial precipitation. *Climate Dyn.*, **38**, 985–1001, https://doi.org/10.1007/s00382-011-1038-9.

——, S. K. Behera, Y. Masumoto, B. Taguchi, H. Sasaki, and T. Yamagata, 2013: Multiple causes of interannual sea surface temperature variability in the equatorial Atlantic Ocean. *Nat. Geosci.*, **6**, 43–47, https://doi.org/10.1038/ngeo1660.

Rodríguez-Fonseca, B., I. Polo, J. García-Serrano, T. Losada, E. Mohino, C. R. Mechoso, and F. Kucharski, 2009: Are Atlantic Niños enhancing Pacific ENSO events in recent decades? *Geophys. Res. Lett.*, **36**, L20705, https://doi.org/10.1029/2009GL040048.

Rong, X., R. Zhang, and T. Li, 2010: Impacts of Atlantic sea surface temperature anomalies on Indo-East Asian summer monsoon–ENSO relationship. *Chin. Sci. Bull.*, **55**, 2458–2468, https://doi.org/10.1007/s11434-010-3098-3.

Ruprich-Robert, Y., R. Msadek, F. Castruccio, S. Yeager, T. Delworth, and G. Danabasoglu, 2017: Assessing the climate impacts of the observed Atlantic multidecadal variability using the GFDL CM2.1 and NCAR CESM1 global coupled models. *J. Climate*, **30**, 2785–2810, https://doi.org/10.1175/JCLI-D-16-0127.1.

Saji, N. H., and T. Yamagata, 2003: Structure of SST and surface wind variability during Indian Ocean dipole mode events: COADS observations. *J. Climate*, **16**, 2735–2751, https://doi.org/10.1175/1520-0442(2003)016<2735:SOSASW>2.0.CO;2.

Saravanan, R., and P. Chang, 2000: Interaction between tropical Atlantic variability and El Niño–Southern Oscillation. *J. Climate*, **13**, 2177–2194, https://doi.org/10.1175/1520-0442(2000)013<2177:IBTAVA>2.0.CO;2.

Smith, R., and Coauthors, 2010: The Parallel Ocean Program (POP) Reference Manual. 141 pp., https://www.cesm.ucar.edu/models/cesm1.0/pop2/doc/sci/POPRefManual.pdf.

Su, J., R. Zhang, T. Li, X. Rong, J.-S. Kug, and C.-C. Hong, 2010: Causes of the El Niño and La Niña amplitude asymmetry in the equatorial eastern Pacific. *J. Climate*, **23**, 605–617, https://doi.org/10.1175/2009JCLI2894.1.

Wang, C., L. Zhang, S.-K. Lee, L. Wu, and C. R. Mechoso, 2014: A global perspective on CMIP5 climate model biases. *Nat. Climate Change*, **4**, 201–205, https://doi.org/10.1038/nclimate2118.

Wang, L., J.-Y. Yu, and H. Paek, 2017: Enhanced biennial variability in the Pacific due to Atlantic capacitor effect. *Nat. Commun.*, **8**, 14887, https://doi.org/10.1038/ncomms14887.

Wu, B., T. Zhou, and T. Li, 2017a: Atmospheric dynamic and thermodynamic processes driving the western North Pacific anomalous anticyclone during El Niño. Part I: Maintenance mechanisms. *J. Climate*, **30**, 9621–9635, https://doi.org/10.1175/JCLI-D-16-0489.1.

——, ——, and ——, 2017b: Atmospheric dynamic and thermodynamic processes driving the western North Pacific anomalous anticyclone during El Niño. Part II: Formation processes. *J. Climate*, **30**, 9637–9650, https://doi.org/10.1175/JCLI-D-16-0495.1.

Wu, R., and Z. He, 2019: Northern tropical Atlantic warming in El Niño decaying spring: Impacts of El Niño amplitude. *Geophys. Res. Lett.*, **46**, 14 072–14 081, https://doi.org/10.1029/2019GL085840.

——, M. Lin, and H. Sun, 2020: Impacts of different types of El Niño and La Niña on northern tropical Atlantic sea surface temperature. *Climate Dyn.*, **54**, 4147–4167, https://doi.org/10.1007/s00382-020-05220-7.

Xie, S.-P., and J. A. Carton, 2013: Tropical Atlantic variability: Patterns, mechanisms, and impacts. *Earth's Climate: The Ocean–Atmosphere Interaction, Geophys. Monogr.*, Vol. 147, Amer. Geophys. Union, 121–142.

Xu, Z., P. Chang, I. Richter, W. Kim, and G. Tang, 2014: Diagnosing southeast tropical Atlantic SST and ocean circulation biases in the CMIP5 ensemble. *Climate Dyn.*, **43**, 3123–3145, https://doi.org/10.1007/s00382-014-2247-9.

Yu, J., T. Li, Z. Tan, and Z. Zhu, 2016: Effects of tropical North Atlantic SST on tropical cyclone genesis in the western North Pacific. *Climate Dyn.*, **46**, 865–877, https://doi.org/10.1007/s00382-015-2618-x.

Zebiak, S. E., 1993: Air–sea interaction in the equatorial Atlantic region. *J. Climate*, **6**, 1567–1586, https://doi.org/10.1175/1520-0442(1993)006<1567:AIITEA>2.0.CO;2.